DEUTERON AND TRITON INDUCED LIGHT ION REACTIONS PRODUCED VIA HIGH-POWER SHORT-PULSE LASERS

By

Andrew O. Bo

A thesis submitted in partial fulfillment of the
requirements for the degree of

Bachelor of Science

Houghton University

May 2026

Signature of Author……..
Department of Physics
May 6, 2026

……
Dr. Mark Yuly
Professor of Physics
Research Supervisor

……
Dr. Brandon Hoffman
Professor of Physics

DEUTERON AND TRITON INDUCED LIGHT ION REACTIONS PRODUCED VIA HIGH-POWER SHORT-PULSE LASERS

By

Andrew O. Bo

Submitted to the Department of Physics
on May 6, 2026 in partial fulfillment of the
requirement for the degree of
Bachelor of Science

Abstract

Light ion and neutron nuclear reactions can be induced via Inertial Confinement Fusion (ICF) and Target Normal Sheath Acceleration (TNSA) using high-power, short-pulse lasers like the OMEGA-60 and OMEGA-EP lasers at the Laboratory for Laser Energetics. In order to measure these reactions, the Short-Lived Isotope Counting System (SLICS) was developed. SLICS can be inserted into the OMEGA-60 and OMEGA-EP target chambers using a Ten Inch Manipulator (TIM). As an initial test of the SLICS detector, TNSA deuterons struck a natural lithium target to induce ^{7}Li(d,p)^{8}Li reactions. SLICS then counted the beta decays from the ^{8}Li product nuclei to calculate the ^{8}Li yield, to which predicted yields, calculated using previously measured ^{7}Li(d,p)^{8}Li cross-sections, were compared. The TIM based SLICS is now a standard diagnostic for experiments on OMEGA-60 and OMEGA-EP.

Thesis Supervisor: Dr. Mark Yuly
Title: Professor of Physics

This material is based upon work supported by the Department of Energy [National Nuclear Security Administration] University of Rochester "National Inertial Confinement Program" under Award Number(s) DE-NA0004144.

TABLE OF CONTENTS

TABLE OF FIGURES

Chapter 1

INTRODUCTION TO LASER INDUCED REACTIONS

1.1. Overview

This thesis describes an experiment performed as an initial test of the Ten-Inch Manipulator (TIM) based Short-Lived Isotope Counting System (SLICS) using Target Normal Sheath Accelerated (TNSA) deuterons from the OMEGA-EP laser at the Laboratory for Laser Energetics (LLE). The ultimate goal is to measure unknown cross-sections of light ion reactions important for understanding astrophysical phenomena such as stellar and Big Bang nucleosynthesis

1.2. Light Ion Reactions

Current nucleosynthesis models require accurate measurements of low energy, light ion cross-sections, which are proportional to the probability of the reaction occurring. Nucleosynthesis is the process where smaller nuclei react to form larger nuclei. When this process occurs in the early universe after the Big Bang it is called Big Bang nucleosynthesis, and when it occurs in stars, stellar nucleosynthesis.

Figure 1 shows the results of such a model of the relative abundances of each isotope after the Big Bang, created by taking the cross-sections of reactions occurring at the given temperature to determine the abundance of each isotope over time. As time increases and temperature decreases, protons and neutrons no longer have enough energy to immediately rip apart when they collide, and so nucleosynthesis occurs as they start sticking together to form larger nuclei. Protons and neutrons will stick together to form deuterons, then, as the temperature further decreases, tritons and ^{3}He will form, then even heavier isotopes like ^{6}Li. Once the universe has cooled down to about 100 keV, nuclei like ^{3}He become much more abundant, and heavier nuclei like ^{6}Li and ^{7}Li begin to form.

In order for these models to be accurate, these low energy reaction cross-sections must be known. Unfortunately, there are some disagreements in the observed and predicted abundances of some elements like Li. ^{7}Li/H was predicted [1] to be (4.391-5.018) x 10^{-10}

whereas the observed relative abundance was (1.58 ± 0.31) x 10^{-10} [2]. This discrepancy of almost a factor of three affects not only the prediction for lithium, but also the abundances of all ensuing reactions, further reducing the accuracy of the model.

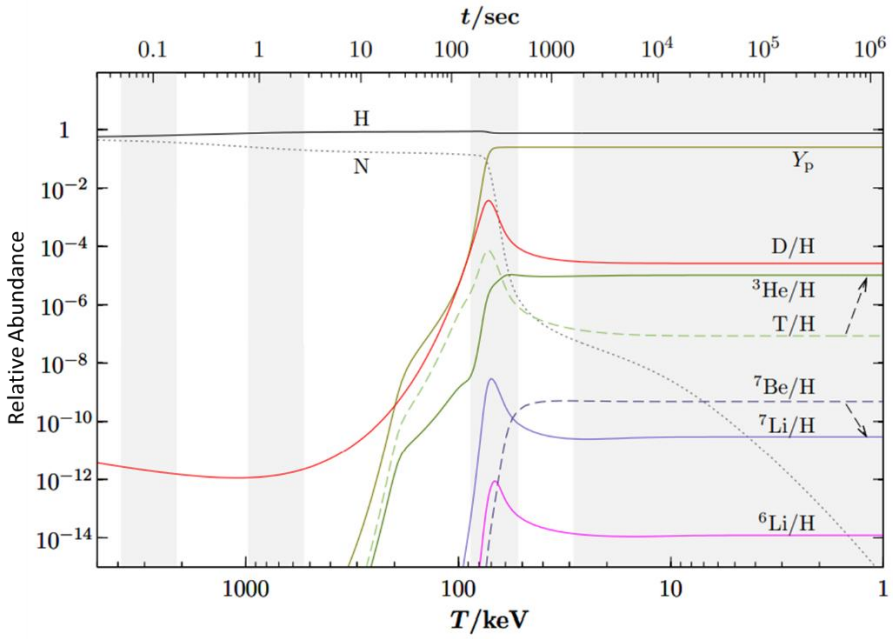

Figure 1. A plot of isotope abundances after the Big Bang with each curve representing the relative abundance of each isotope over time. The grey bands are the primary stages of Big Bang Nucleosynthesis, from left to right: neutrino decoupling, electron-positron annihilation and n/p freeze-out, D bottleneck, and freeze-out of all nuclear reactions. The 30 keV -100 keV D bottleneck band is where heavier isotopes like ^{6}Li and ^{7}Li start to form. Figure modified from Ref [3].

These models are based off predictions and extrapolations of the cross-sections that disagree with the measured cross-sections. In Figure 2, cross-section measurements are compared to cross-sections produced by the prediction code TALYS-1.9 [4] and S-factor extrapolations [5]. In the energy ranges where the cross-section was measured, the TALYS predictions do not match the measurements, and the S-factor extrapolates past the lowest energy cross-sections that have been measured. These models, in the figure, are based on cross-sections at even higher energies, with discrepancies already present at these lower, but still too high, energies.

As discussed later, the lack of low energy measurements is due to particle accelerators, which has been the primary method of making these measurements, only being able to measure cross-sections down to about 100 keV, while for Big Bang nucleosynthesis, as seen in Figure 1, the reactions occur between 30-100 keV, and stellar reactions occur between 1-100 keV [6]. Additionally, due to tritium being radioactive, most tritium reactions, like the T-T reaction, have few, if any, previous measurements [7].

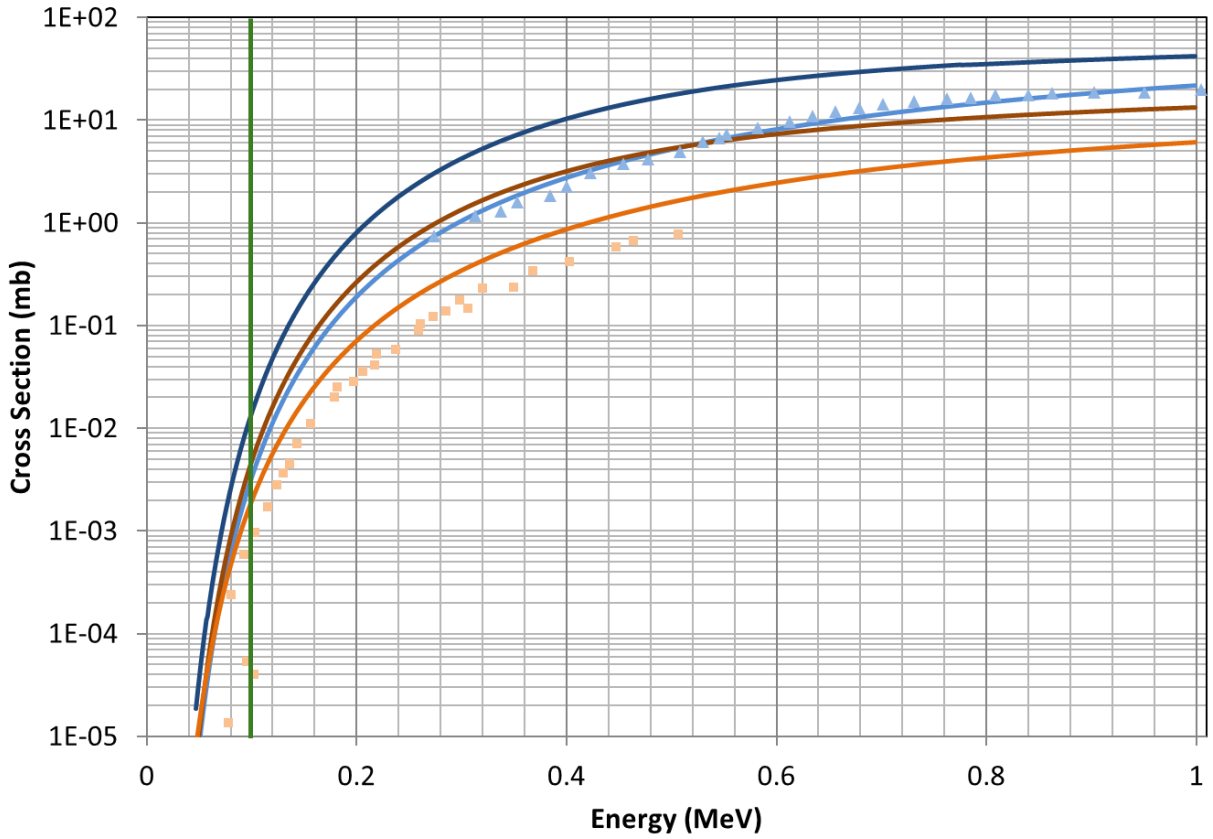

Figure 2. Extrapolated cross-sections. The ^{6}Li(t,p)^{8}Li cross-sections are predicted by TALYS-1.9 [4] (dark blue curve), S-factor [5] (light blue curve), and measured (light blue triangles), and ^{7}Li(t,α)^{6}He predicted by TALYS (brown curve), S-factor (orange curve), and measured (orange squares). Particle accelerators are typically only able to measure reactions down to ~0.1 MeV (green line). Figure adapted from Ref [8].

1.3. High-Power Short-Pulse Laser Induced Reaction Methods

1.3.1. Problems with Accelerator Experiments

Traditionally, a particle accelerator would be used to make cross-section measurements for these models. In a particle accelerator experiment, a beam of incident particles is directed at

a nuclear target causing nuclear reactions to occur, of which the resulting product nuclei may be radioactive. Figure 3 shows, for an example case, the number of product nuclei as a function of time from a particle accelerator beam with constant current striking a target creating radioactive nuclei at a constant rate. The nuclei decay at a rate proportional to the number of activated nuclei present in the target, so as time increases, the rate of decay increases, while the rate of creation remains constant. Eventually the decay rate approaches the rate of creation, so the nuclei are decaying just as fast as they can be created. This causes the number of product nuclei to asymptotically approach a maximum. As it approaches the maximum number of product nuclei, the beam must be shut off, so the decays can be counted to determine this maximal value, which can then be used to find the cross-section. This process of building up target nuclei then allowing them to decay must be repeated numerous times until a statistically significant number of decays have been counted. During this time, background is also able to accumulate. For small cross-sections, this must be repeated even more times to achieve a statistically significant number of decays detected, leading to a further increase in background accumulated, further exacerbating the problem.

Another problem with using particle accelerators is that it is very difficult to measure cross-sections below ~100 keV. Since incident particles are striking a target, they lose energy as they pass through the target until they exit or stop. As the initial energy of the incident particles is decreased, the distance they can travel through the target also decreases, resulting in interactions in only a very thin slice.

Additionally, accelerators that accelerate tritium, which is radioactive, become contaminated [9], which eventually necessitates decommissioning them [10]. For this reason, very few accelerator experiments have been carried out with a tritium beam, and for many decades there were no active labs producing a primary triton beam [7]. Recently, Florida State University started upgrading a tandem accelerator to produce a 4-17 MeV 20 nA triton beam [11].

1.3.2. Laser Experiments at the Laboratory for Laser Energetics

In comparison with accelerator experiments, using high-power short-pulse lasers can decrease the background collected possibly lower the energies that can be measured, and

handle tritium without being contaminated. Laser experiments can be performed at the Laboratory for Laser Energetics (LLE), a laboratory operated by the University of Rochester, for the department of energy, in upstate New York. LLE researches using high-power ultra-fast lasers. LLE has three laser systems, OMEGA-60, OMEGA-EP, and MTW. OMEGA-60 is used to create thermonuclear reactions by shooting a macroscopic target isotropically with 60 lasers. The OMEGA-60 chamber is specially equipped to handle tritium, allowing these reactions to be measured. OMEGA-EP can be used to accelerate ions towards a nuclear target. The OMEGA-EP lasers can be redirected into the OMEGA-60 chamber allowing TNSA tritium experiments to be performed. MTW is a smaller, less powerful laser that allows lower energy TNSA experiments to be performed at a lower cost with a higher shot rate.

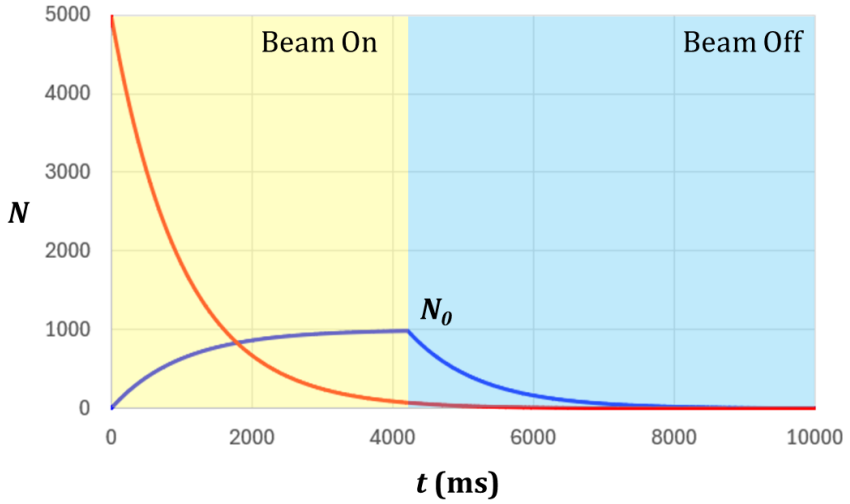

Figure 3. The number of product nuclei (N) produced by a particle accelerator (blue) and ultra-fast high-power laser acceleration (red) (such as TNSA) over time for an example case. For the accelerator, the beam is turned on (yellow shaded) until there nearly reaches a point of equilibrium, N_0, where the rate of creation is about the same as the rate of creation. At this point the accelerator is turned off (blue shaded) and decays are counted. For TNSA, the products are created so quickly that essentially none have decayed until after the laser pulse, allowing the number to be counted immediately after the shot. Figure adapted from Ref [12].

1.3.3. Target Normal Sheath Acceleration

The first of the two methods of using lasers to circumvent these problems is Target Normal Sheath Acceleration (TNSA) [7]. In Figure 4, a laser pre-pulse strikes a laser target with the desired nuclei adsorbed onto the face of the target, creating a plasma. When the main high-

power short laser pulse reaches the target, the energy is transferred to the plasma electrons, blasting them off the target. This creates an electric field that accelerates the ions (10^{12} –10^{13} using OMEGA-EP [13]) on the surface of the laser target towards a nuclear target such that they all strike the nuclear target within a few nanoseconds [7], before essentially any product nuclei are able to decay. Since all of the product nuclei are created nearly simultaneously, this greatly reduces both the time required to perform an experiment and consequently the number of background counts collected. This means reactions with small cross-sections that would otherwise be difficult to measure can be measured. Like the particle accelerator experiments, TNSA, is unable to measure low energy cross-sections, as any ions with less than ~100 keV will only interact with a very thin slice of the target making it difficult to obtain a statistically significant number of reactions.

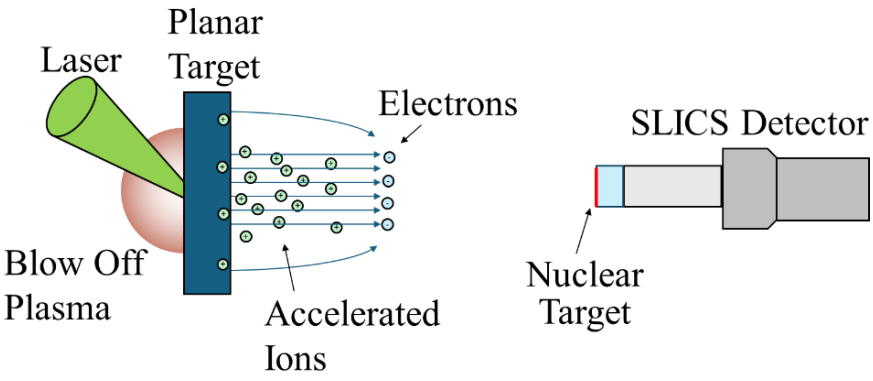

Figure 4. The TNSA Process. In TNSA, a laser strikes a laser target which creates a plasma that blasts off the electrons. This creates an electric field that accelerates the desired ions on the surface of the laser target towards a nuclear target, inducing the desired nuclear reaction. Figure taken from Ref [6].

1.3.4. Inertial Confinement Fusion

In the second method, Inertial Confienment Fusion (ICF), a macroscopic (about 1 mm diameter) target capsule composed of a thin plastic shell filled with deuterium (d or ^{2}H), tritium (t or ^{3}H), or a mixture of the two, that is possibly cryogenically frozen, is shot isotropically by sixty high-energy short-pulse lasers in the case of OMEGA-60. This causes the plastic shell to ablate and blow off, compressing the nuclear fuel contained within. This sudden compression creates a hot, dense plasma where reactant nuclei can undergo nuclear

reactions. If the plasma is hot and dense enough, the reactions can become self-sustaining, which is called ignition, and a significant fraction of the nuclei will be able to react.

There are two ways ICF can be used to measure cross-sections. In the first, depicted in Figure 5, when the target capsule nuclei undergo D-T reactions, a large number (~10^{14}) of 14.1 MeV neutrons are created via $^{2}H(t,n)^{4}He$. These neutrons can strike a nuclear target placed on the end of a detector, where they have a chance of causing nuclear reactions. Like TNSA, this is primarily beneficial for creating a large number of product nuclei in the nuclear target all at once.

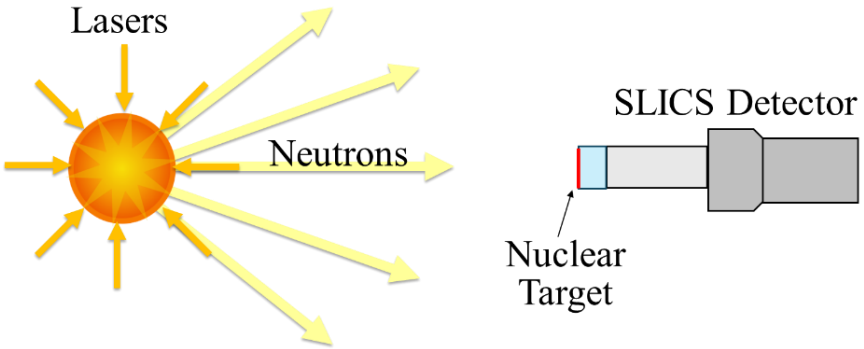

Figure 5. Diagram showing primary ICF neutrons. Neutrons from the reaction strike a nuclear target on a detector, causing nuclear reactions to occur. Neutrons from a D-T fusion reaction are 14.1 MeV. Figure taken from Ref [6].

Another way to use ICF to measure reaction cross-sections, depicted in Figure 6, is by doping the target capsule with a small amount of another isotope, for example 1% ^{7}Li. Nuclear reactions occur in the hot spot after the laser shot, then the plasma expands, cools, and eventually forms an expanding neutral gas that includes the reaction products from the dopant, in this case ^{8}Li from the reaction $^{7}Li(d,p)^{8}Li$, which may stick to a getter foil on the end of the detector. During an ICF shot, the reactions occur in the hot dense plasma at around 20 keV or below. Because these are thermonuclear reactions taking place in a well-mixed plasma involving a huge number of reactant nuclei in a tiny volume, rather than incident particles penetrating a target, reactions at energies much lower than the approximate 100 keV limit of a particle accelerator can be measured. These low energy reactions can be

found in stars, which also take place in similar plasmas, and the early universe shortly after the Big Bang.

Some ICF target chambers, like the OMEGA-60, are specially equipped to handle tritium. Using a doped ICF shot with a getter foil may allow unknown tritium cross-sections to be measured. Likewise, performing a joint shot, using the OMEGA-EP lasers with the OMEGA-60 chamber, allows the creation of TNSA tritons, which is another viable option to measure tritium reaction cross-sections above ~100 keV.

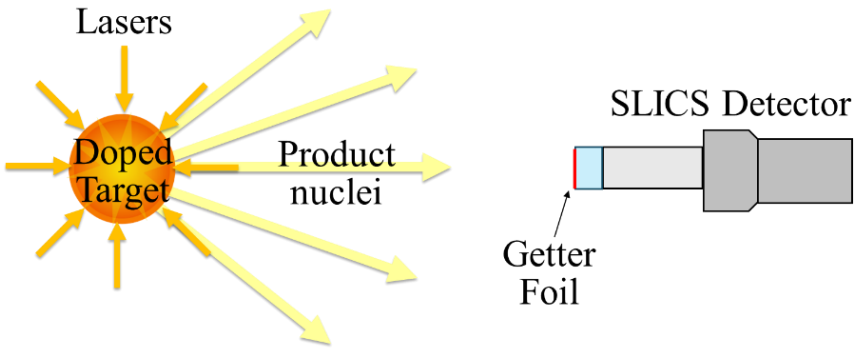

Figure 6. Diagram showing ICF doped target. Product nuclei from thermonuclear reactions in a doped target strike and stick to a getter foil on the end of a detector, where they stick and then decay. Figure taken from Ref [6].

1.4. Short-Lived Isotope Counting System

In order to make these laser induced cross-section measurements, the Short-Lived Isotope Counting System (SLICS) was developed. SLICS detects the beta decays of the product nuclei. Figure 7 shows the light ions on the chart of nuclides, particularly highlighting those that beta decay with half-lives from 10ms to 20s. The SLICS was designed to measure these isotopes.

1.4.1. How the Short-Lived Isotope Counting System Works

The SLICS is a phoswich detector telescope consisting of a thin fast (dE) and a thick slow (E) scintillator. Figure 8 shows a beta particle, from a ^{8}Li decay, passing through SLICS. The beta particle enters the dE and E scintillators, loses energy, and emits an amount of light proportional to the energy lost in each. This light travels down a glass lightguide into a

photomultiplier tube (PMT) which converts the light to an electrical pulse. Because of the differences in the scintillator decay time, the individual dE and E signals can be separated electronically. Figure 9 shows a 2D histogram of the energy lost in each scintillator. The particle can be identified based on the region of the graph in which it falls, with beta events falling primarily in the region outlined in red. A Particle Time-of-Flight (pTOF) detector can be added to the SLICS detector for TNSA experiments to determine the incident ion energy spectrum.

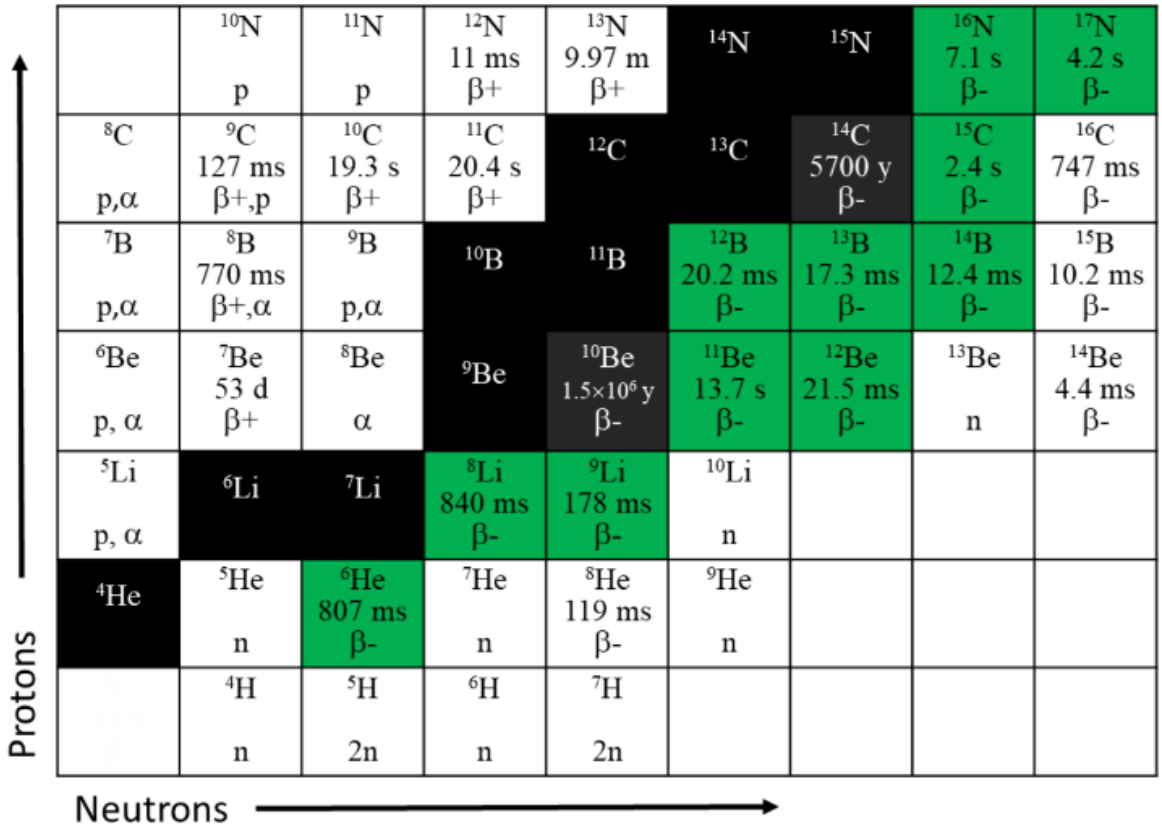

Figure 7. Chart of nuclides. SLICS is designed to measure light ion beta decays with half-lives from 10ms to 20s (green). SLICS can be used to measure reactions that create any of these isotopes as product nuclei. Figure taken from Ref [6].

1.4.2. TIM Based SLICS

The SLICS was designed to fit in a Ten Inch Manipulator (TIM) that allows the SLICS to be inserted directly into the OMEGA-60 and OMEGA-EP laser chambers at LLE. This allows it to be used as a diagnostic for ICF capture experiments where product nuclei stick to a getter

foil on the face of the detector and TNSA experiments where TNSA ions strike a target on the face of the detector. Figure 10 is an exploded diagram of the TIM-based SLICS. The main body of the SLICS is inside a bubble housing allowing the PMT to remain at atmosphere while the chamber is in a vacuum in order to prevent sparking. Likewise, the high-voltage cables are in a tube kept at atmosphere. The carrier chain assembly allows the SLICS to be inserted and retracted as needed for a given shot without having to remove the whole assembly.

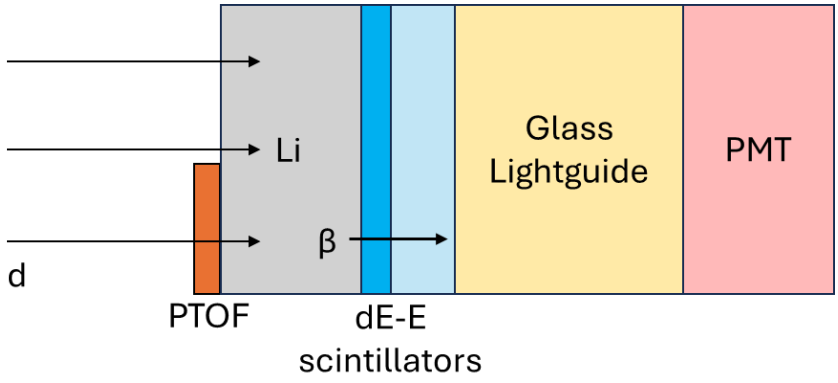

Figure 8. A schematic diagram of SLICS. Deuterons strike a thin target, such as a lithium film, creating radioactive product such as ^{8}Li, which beta decays. The resulting betas pass through the phoswich detector, emitting light from the dE and E scintillators. The light from each scintillator passes down the lightguide into the PMT. A pTOF detector is placed on the front of the detector to measure the energy spectrum of the incident deuterons.

This TIM-based design is a prototype diagnostic for the proposed NSF-OPAL laser [14]. NSF-OPAL is a proposed laser system designed for high shot-rate experiments. The high shot rate will allow for more shots to be performed each day for an experiment, which will improve the result statistics. Additionally, if provided with a tritium capable chamber, this will eliminate the need for a joint shot for tritium using the OMEGA-EP lasers to produce a TNSA triton beam in the OMEGA-60 chamber which is able to handle tritium. One of the proposed flagship NSF-OPAL experiments is measuring the ^{7}Li(t,γ)^{10}Be and ^{7}Li(t,n)^{9}Be reactions using the SLICS detector.

1.5. SLICS Experiments

The TIM-based SLICS detector is the culmination of many feasibility experiments with multiple prototype detectors.

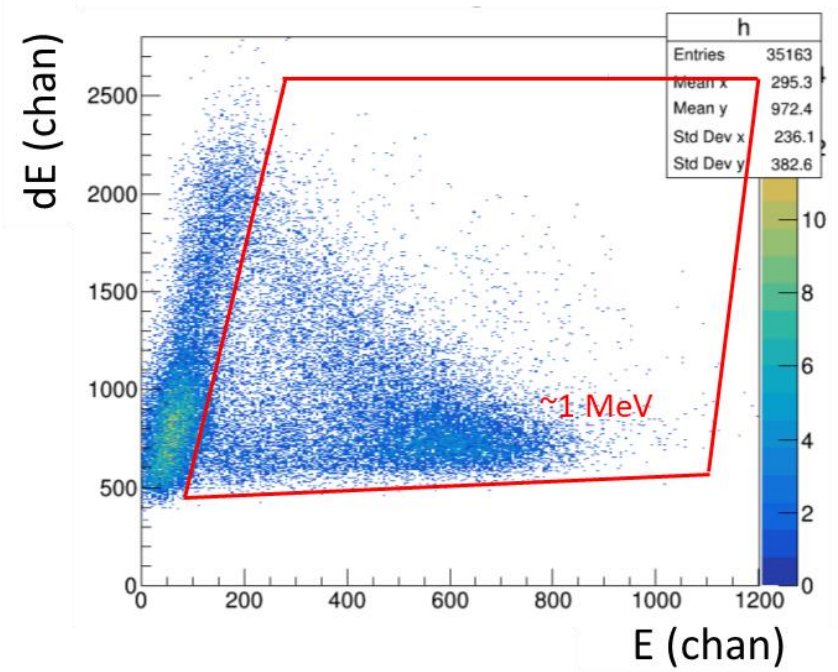

Figure 9. A ^{207}Bi calibration plot for SLICS. The 2D histogram from SLICS of the energy lost in the E (horizontal axis) and dE (vertical axis) layers where the color of each bin is the number of events at that energy, with blue being less and orange being more. ^{207}Bi emits a beta spectrum as well as a monoenergetic peak used to calibrate the channels to energy. Inside the region outlined in red is where the good ^{8}Li beta events will fall. The band to the left of the box is particles that lose all of their energy in the dE layer and are stopped before reaching the E layer, along with beta particles at extreme angles that only pass through the dE layer.

1.5.1. ^{9}Be(n,α) ^{6}He with Silicon Detector (2016)

In 2016, an experiment [15] was carried out to create and detect ^{6}He as an initial step towards measuring the reaction ^{3}H(t,γ)^{6}He, which occurs during ICF, but whose cross-section has never been previously measured. In order to do this, a silicon detector telescope was created with a dE and E layer. The SUNY Geneseo Pelletron accelerator was used to create neutrons from the ^{2}H(d,n)^{3}He reaction. The neutrons then struck a beryllium target causing the reaction ^{9}Be(n,α)^{6}He. Beta decays were counted and the half-life for ^{6}He was measured to be 818 $\pm$ 18 ms, which agrees with the previously measured 807 ms.

1.5.2. ^{9}Be(n,α) ^{6}He with Phoswich Detector (2017)

Unfortunately, the silicon detector would not survive an ICF shot. So, in 2017, the detector was redesigned [15] using plastic scintillators, with decay constants of 2 ns and 285 ns for

the dE and E layers respectively, to create the first primitive version of SLICS, a phoswich detector. The experiment from 2016 was then repeated using the new detector at SUNY Geneseo to create ^{6}He via the reaction ^{9}Be(n,α)^{6}He. This time, the half-life was measured to be 789 $\pm$ 38 ms, meaning the new detector was also a viable means to make these measurements.

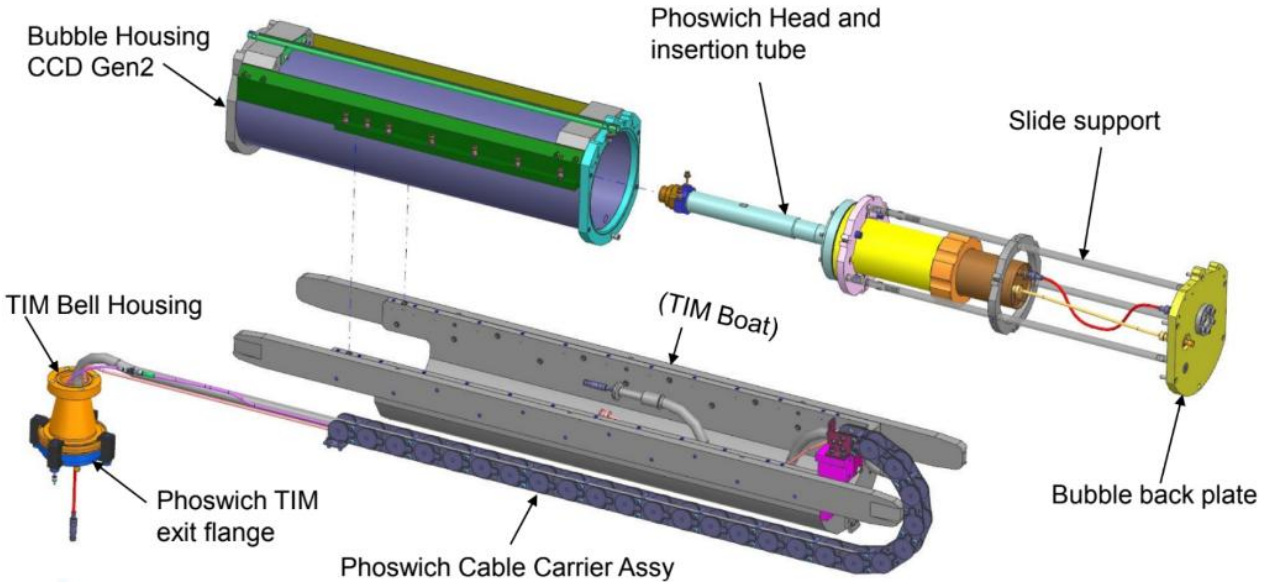

Figure 10. The TIM based SLICS detector. An exploded schematic of the TIM based phoswich detector. The SLICS fits inside a bubble housing that keeps the PMT and HV cables at atmosphere to prevent sparking. The cable carrier assembly allows for easy insertion and retraction into the OMEGA-60 and OMEGA-EP chambers. A removable pTOF detector (not shown) can be attached for TNSA experiments. Figure taken from Ref [6].

1.5.3. ^{40}Ar(d,p)^{41}Ar Experiment (2018)

Since ^{6}He is an inert gas, a method was proposed to trap the gas, using a turbopump, after an ICF implosion, then use the SLICS to measure the decays of the trapped nuclei. In 2018, in order to test this [8], ^{41}Ar, another inert gas with similar decay energies, was created via ^{40}Ar(d,p)^{41}Ar by using the SUNY Geneseo accelerator to accelerate deuterons into a ^{40}Ar gas cell. Unlike ^{6}He's half-life of 807 ms, ^{41}Ar has a half-life of 109 min, so it could be created at Geneseo, then transported to Houghton University. When ^{41}Ar was released into a test chamber at Houghton via a fast valve, multiple fast ion gauges were used to measure the pressure change across the large vacuum chamber. The ^{41}Ar gas was then trapped using a turbopump and a silicon surface barrier detector was used to count the beta decays. The half-

life was determined to be 109.9 $\pm$ 6.6 min, meaning this is a viable means to trap and make these measurements

1.5.4. 4π Detector (2019)

Just like in the ^{9}Be(n,α) ^{6}He experiments, the detector from the ^{40}Ar(d,p)^{41}Ar experiment was redesigned [16] to be a hollow rectangular prism with phoswich scintillators for walls. After an ICF shot, the inert gas would be trapped, using a turbopump, inside the detector which would then be able to count the decays in the gas. Due to the gas being inside the detector, the decays were measured from every direction, or a 4π steradian solid angle, hence the name: 4π detector.

1.5.5. ICF Ride-Along (2019)

In order to make these measurements, the detectors must be able to count the decaying isotopes of interest over the intense background after the laser shot. In 2019, a ride-along experiment [16] was performed outside the OMEGA-60 chamber at LLE. Both the SLICS and the 4π detector were placed in the webbing outside the OMEGA-60 laser chamber during multiple high-yield D-T target shots. The maximum total count rate of the background for the 4π detector was found to be too high to work without additional shielding, whereas the SLICS count rate was found to be workable.

1.5.6. Exploding Wire Experiment (2021, 2022)

In experiments in 2021 [17] and 2022 [18], a radioactive isotope was created and vaporized to simulate trapping the radioactive gas formed after an ICF shot. In 2021, a deuteron beam from the SUNY Geneseo accelerator struck a copper film that was electroplated onto a tungsten filament causing ^{65}Cu(d,p)^{66}Cu to occur. A large pulse of current was used to heat and rapidly evaporate the copper atoms, which then drifted and stuck to the getter foil on the end of the SLICS detector, allowing the decays to be counted. This experiment was repeated in 2022 using fluorine, to cause ^{19}F(d,p)^{20}F, and lithium, which is one of the light ions of interest, to cause ^{7}Li(d,p)^{8}Li. Using this method, the SLICS captured and detected between 1.0-1.7% of the ^{8}Li created, which indicates that a statistically significant number of decays could be detected during an ICF shot when measuring a small cross-section.

1.5.7. MTW Experiment (2023)

In 2023 a proof-of-concept experiment [12,19,20] was conducted using the Multiterawatt (MTW) laser at the Laboratory for Laser Energetics to test whether it might be possible to make light-ion cross section measurements using TNSA with SLICS. A laser pulse from MTW struck a deuterated-polyethylene laser target accelerating TNSA deuterons, whose energies were measured using the Thomson Parabola Ion Spectrometer (TPIS) and the pTOF. The deuterons struck a natural lithium target placed just upstream of the SLICS causing ^{7}Li(d,p)^{8}Li. The ^{8}Li beta decays were counted, and the measured yield was within a factor of two of the predicted value using previously measured cross-sections, demonstrating that it is possible to perform these measurements using TNSA.

1.5.8. Efficiency (2024)

The SLICS is unable to detect every beta decay, only the beta particles that lose energy passing through the scintillators are counted. In order to account for this, an experiment [12] was conducted in 2024 at SUNY Geneseo to measure the efficiency for ^{8}Li created at different locations across the face of the detector, shown in Figure 11, which were then integrated to find the total efficiency of the detector. The efficiency is the ratio of betas that were detected to number of betas that hit the detector. Using the 1.7 MeV Pelletron particle accelerator a beam of deuterons struck a natural lithium target creating ^{8}Li via the reaction ^{7}Li(d,p)^{8}Li. The ^{8}Li beta decays were counted using the SLICS detector. A silicon detector was used to detect the α particles from the reaction ^{6}Li(d,α)^{4}He. Then, using the known ^{6}Li(d,α)^{4}He cross-section and ^{6}Li/^{7}Li ratio in natural lithium, the amount of ^{7}Li was determined. The known ^{7}Li(d,p)^{8}Li cross-section, along with the beam current, was used to determine the number of ^{8}Li created. The beam current was measured by elastically scattering the deuteron beam at a 90-degree angle off a thin gold foil, using the known ^{197}Au(d,d)^{197}Au scattering cross-section. A camera was used to determine the beam position on the face of the detector.

GEANT4 [21] was used to simulate the SLICS detector's efficiency. To do this, a ^{8}Li point source was placed on the face of the simulated phoswich at a given radius, and after 1 million events, the fraction of events that lost energy in, and were thus detected by, the simulated detector geometry was the efficiency at that radius. This was repeated at points across the

face of the detector and integrated to get the total efficiency. Figure 11 shows the simulation agreed with the data collected from SUNY Geneseo.

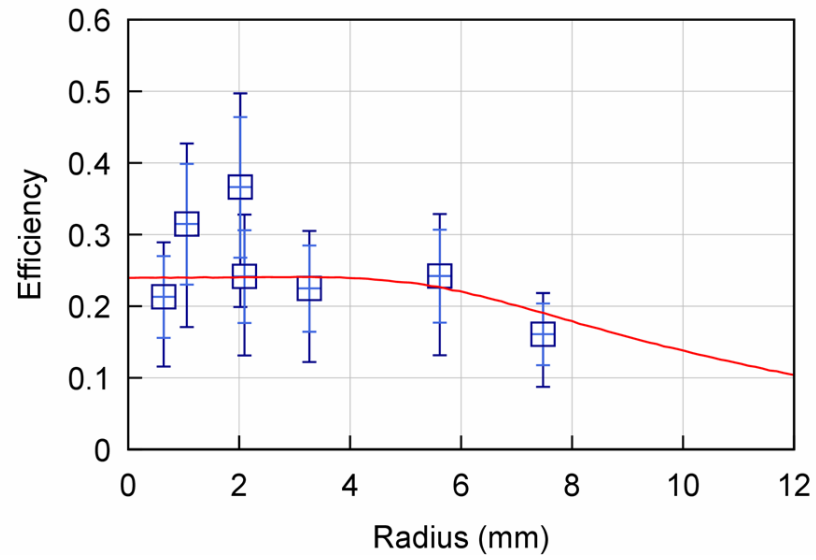

Figure 11. The ^{8}Li detection efficiency as a function of distance from the center of the SLICS detector. The blue squares are the measured efficiency of the SLICS detector. The error bars are due to the spread in the previously measured ^{7}Li(p,α)^{4}He cross-section used to calculate target thickness (dark blue) and the range in previously measured cross-sections of ^{7}Li(d,p)^{8}Li at 1.5 MeV (light blue). The red curve shows the efficiency predicted by the GEANT4 simulation as a function of distance from the center. Figure taken from Ref [12].

1.6. OMEGA-EP Experiment

This thesis describes an initial test of the TIM-based SLICS carried out using the OMEGA-EP laser, shown in Figure 12, which consisted of two independent lasers, the sidelighter and the backlighter. The sidelighter laser was shot at a deuterated stainless-steel substrate, creating TNSA deuterons that struck a ~5 μm thick oxidized natural lithium target placed on the front of the SLICS causing ^{7}Li(d,p)^{8}Li. The pTOF was used to measure the deuteron energy spectrum. Alternating with the sidelighter shots, the laser target was rotated 90° so the backlighter, using ostensibly the same laser parameters, could accelerate deuterons towards a Thompson Parabola Ion Energy Analyzer (TPIE). The resulting energy spectrum was compared to the one obtained by the pTOF.

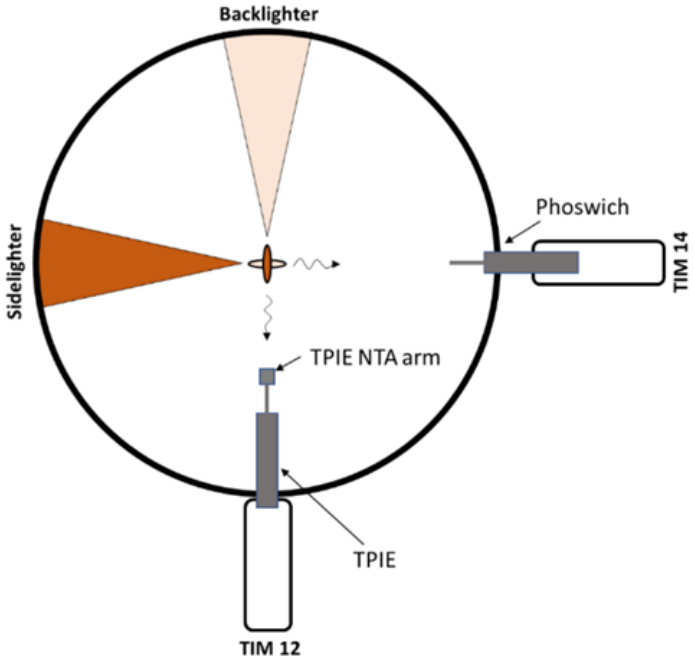

Figure 12. OMEGA-EP Experiment Diagram. The OMEGA-EP made alternating shots between the sidelighter and back lighter lasers. The sidelighter laser struck a deuterated stainless-steel substrate causing TNSA deuterons to strike a thin lithium film on the end of the SLICS causing $^{7}Li(d,p)^{8}Li$. The pTOF was used to estimate the deuteron energy spectrum. The backlighter laser was used to cause TNSA deuterons from a deuterated stainless-steel target to strike the TPIE to obtain the resulting energy spectrum.

Chapter 2

THEORY OF MEASURING NUCLEAR DECAYS

2.1. Nuclear Cross-sections

In the experiment described in this thesis, shown in Figure 12, the OMEGA-EP sidelighter laser was used to accelerate TNSA deuterons towards a lithium target placed directly upstream from SLICS. The TNSA deuterons struck the lithium target, creating ^{8}Li. The SLICS was then used to measure the ^{8}Li yield for the shot. To predict the ^{8}Li yields measured by the SLICS, the laser parameters of the shot, along with the known ^{7}Li(d,p)^{8}Li cross-section was used. To do this, the previously measured cross-section was integrated over the range of incident deuteron energies giving the predicted yield for the shot.

Figure 13 shows incident particles striking a nuclear target causing dN/dt nuclear reactions to occur per time, when the beam spot is larger than the target. If the number of incident particles per area per time, F, is doubled, dN/dt will also double. Likewise, if the number of target nuclei, N_T, is doubled, dN/dt will also double. So, the number of nuclear reactions per time is proportional to F and N_T

$$\frac{dN}{dt} = \sigma(E_0)FN_T, \tag{1}$$

where the cross-section, $\sigma(E_0)$, is the constant of proportionality for incident ions of energy E_0. The number of target nuclei is

$$N_T = \rho TA, \tag{2}$$

where ρ is the density of nuclei per volume, T is the target thickness, and A is the area of the target, which is completely irradiated by the beam.

2.2. Energy Loss and Variation

The previous calculations assume the incident particles are monoenergetic and do not lose energy as they pass through the target; however, this is not the case.

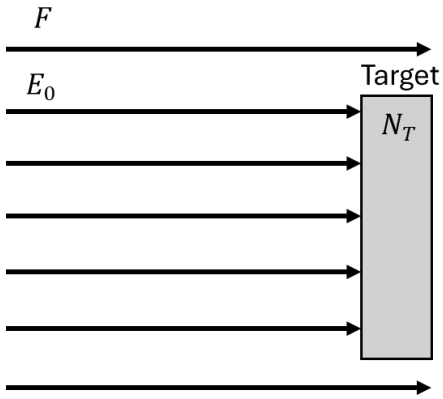

Figure 13. Particles incident on a nuclear target. A beam of F particles per area per time, and energy E_0, strike a target with N_T nuclei, completely irradiating the target. This causes dN/dt reactions to occur per time.

Figure 14 shows a particle passing through a target, losing energy. The distance traveled, dx, by a particle that loses energy, dE, is

$$dx = \frac{1}{\frac{dE}{dx}(E)}\,dE, \tag{3}$$

where dE/dx is the stopping power of the target, which is calculated using the Bethe-Bloch formula [22,23,24]. The particle will stop when it has no energy, so the range of the particle, R, is

$$R = \int dx = \int_{E_0}^{0} \frac{1}{\frac{dE}{dx}(E)}\,dE, \tag{4}$$

for some initial energy E_0.

From Equation (1) and Equation (2), the number of product nuclei created per time, dN_c/dt in a slice of thickness dx is

$$\frac{d^2N_c}{dt}(E,x) = \sigma(E)\mathrm{F}\rho\mathrm{A}\mathrm{dx}. \tag{5}$$

Using Equation (3), this can be rewritten as

$$\frac{d^2N_c}{dt}(E) = F\rho A\frac{\sigma(E)}{\frac{dE}{dx}(E)}dE. \tag{6}$$

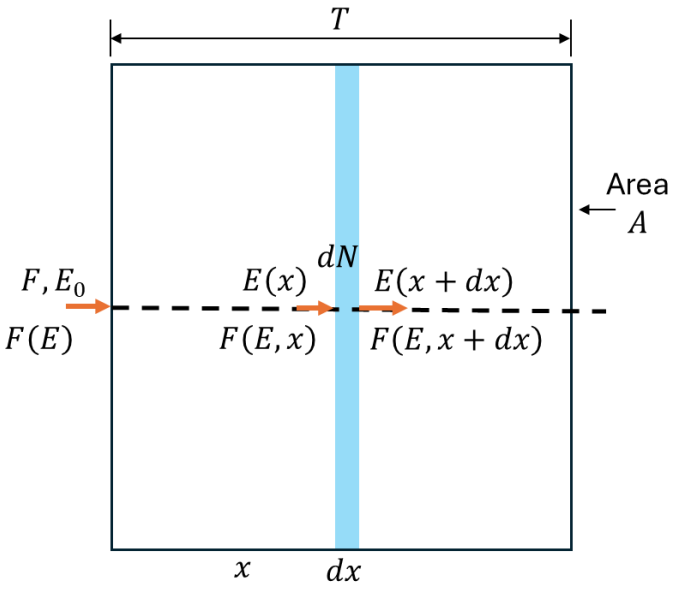

Figure 14. Energy loss in a target. A beam of F particles per area per time strikes a target with area A. If the beam is monoenergetic, the particles have initial energy E_0, and they pass through a distance x losing energy. The particles have energy E(x) as they reach the slice of length dx, where reactions will occur. The particles will leave the slice with energy $E(x + dx)$. If the beam has a distribution of energies, $F(E)$, they will pass through a distance x losing energy. The particles will have energy distribution $F(E, x)$ as they enter the slice of length dx, where reactions will occur. The particles will leave the slice with energy distribution $F(E, x + dx)$.

Integrating this over all the slices gives the total rate,

$$\frac{dN_c}{dt} = F\rho A\int_{E_0}^{E_f}\frac{\sigma(E)}{\frac{dE}{dx}(E)}dE, \tag{7}$$

where E_f is the final energy. If $R \leq T$, then the particle stops before passing all the way through the target, so $E_f = 0$, otherwise, $E_f = E(x = T)$, where $E(T)$ can be determined by solving

$$\int_0^T dx = \int_{E_0}^{E(T)}\frac{dx}{dE}(E)dE. \tag{8}$$

So, the rate of creation is given by

$$\frac{dN_c}{dt} = \begin{cases} F\rho A \int_{E_0}^{0} \frac{\sigma(E)}{\frac{dE}{dx}(E)} dE\,, & R \le T \\ F\rho A \int_{E_0}^{E(T)} \frac{\sigma(E)}{\frac{dE}{dx}(E)} dE\,, & R \ge T \end{cases}, \tag{9}$$

with the number created, N_c, from $t = 0$ to $t = t_f$, given by

$$N_c = \begin{cases} \int_0^{t_f} F\rho A \int_{E_0}^{0} \frac{\sigma(E)}{\frac{dE}{dx}(E)} dE\, dt, & R \le T \\ \int_0^{t_f} F\rho A \int_{E_0}^{E(T)} \frac{\sigma(E)}{\frac{dE}{dx}(E)} dE\, dt, & R \ge T \end{cases}. \tag{10}$$

This gives the number of product nuclei that are created by a beam of monoenergetic incident particles with energy E_0. However, the incident particles will have a distribution of energies. To account for this, integrating the incident energy spectrum, which is the number of incident ions per energy per area per time, $F(E)$, over E gives

$$\frac{dN_c}{dt} = \begin{cases} \rho A \int_0^{\infty} F(E) \int_{E}^{0} \frac{\sigma(E')}{\frac{dE}{dx}(E)} dE'\ dE\,, & R(E) \le T \\ \rho A \int_0^{\infty} F(E) \int_{E}^{E(T)} \frac{\sigma(E')}{\frac{dE}{dx}(E)} dE'\ dE\,, & R(E) \ge T \end{cases}. \tag{11}$$

The total yield, N_c, from $t = 0$ to $t = t_f$, is given by

$$N_c = \begin{cases} \rho A \int_0^{t_f} \int_0^{\infty} F(E) \int_{E}^{0} \frac{\sigma(E')}{\frac{dE}{dx}(E)} dE'\ dE\, dt, & R(E) \le T \\ \rho A \int_0^{t_f} \int_0^{\infty} F(E) \int_{E}^{E(T)} \frac{\sigma(E')}{\frac{dE}{dx}(E)} dE'\ dE\ dt\,, & R(E) \ge T \end{cases}. \tag{12}$$

2.3. Decay and Growth Curves

The SLICS does not detect the prompt radiation from the creation of these reaction products, but the decays of these product nuclei, so the number of product nuclei must be determined from the number of decays detected. As these radioactive product nuclei decay, the rate of decay, dN/dt, is proportional to the number of product nuclei,

$$\frac{dN}{dt} = -\lambda N, \tag{13}$$

where N is the number of product nuclei and λ is a constant of proportionality called the decay constant. Solving this differential equation gives

$$N(t) = N_0 \mathrm{e}^{-\lambda \mathrm{t}}, \tag{14}$$

where N_0 is the initial number of product nuclei. Figure 15 shows an example plot of radioactive product nuclei from a target decaying over time.

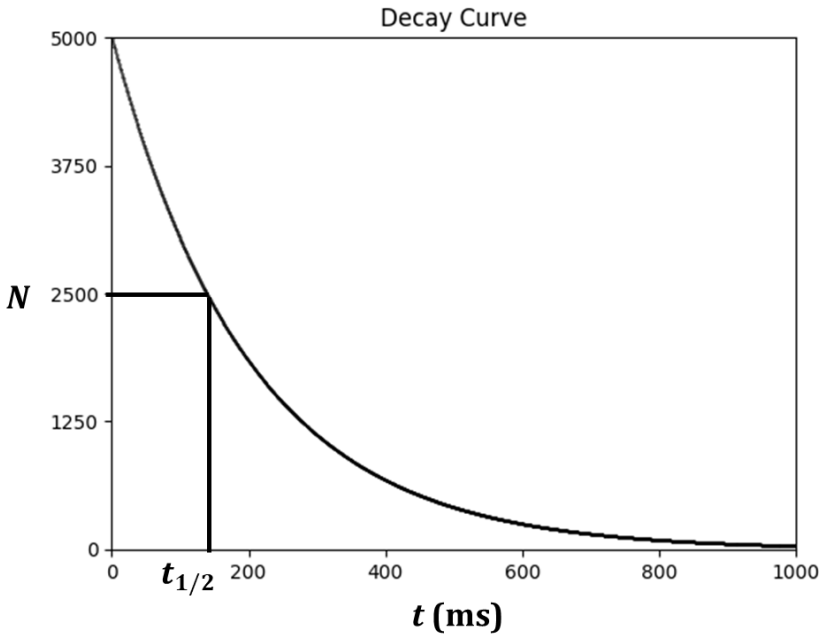

Figure 15. Example decay curve. The number, N, of activated particles in a target decreases as they decay at a rate proportional to the number remaining. The time it takes for the number of activated nuclei to halve is known as the half-life, $t_{1/2}$.

The half-life, $t_{1/2}$, is when half the nuclei have decayed, or

$$N(t_{1/2}) = N_0 e^{-\lambda t_{1/2}} = \frac{N_0}{2}. \tag{15}$$

Thus, the half-life is given by

$$\mathrm{t}_{1/2} = \frac{\ln 2}{\lambda}. \tag{16}$$

If product nuclei are decaying as they are being created, as shown in Figure 16, the total change in product nuclei per time, dN/dt, from both creation in Equation (11) and decay in Equation (13) is

$$\frac{dN}{dt} = \frac{dN_c}{dt} - \lambda N, \tag{17}$$

where the first term gives the rate of creation and the second term gives the rate of decay. Equation (17) can also be written, since dN_c/dt is constant,

$$\mathrm{dt} = \frac{\mathrm{dN}}{\frac{dN_c}{dt} - \lambda N}. \tag{18}$$

This can be integrated to give

$$\mathrm{t} + \mathrm{c} = -\frac{1}{\lambda} \ln \left[\frac{dN_c}{dt} - \lambda N \right], \tag{19}$$

where c is an integration constant. This equivalent to

$$\mathrm{N} = -\frac{1}{\lambda} \left[C e^{-\lambda t} - \frac{dN_c}{dt} \right], \tag{20}$$

where C is a constant. When $t = 0, N = 0$,

$$0 = -\frac{1}{\lambda} \left[C e^{0} - \frac{dN_c}{dt} \right], \tag{21}$$

so

$$C = \frac{dN_c}{dt}. \tag{22}$$

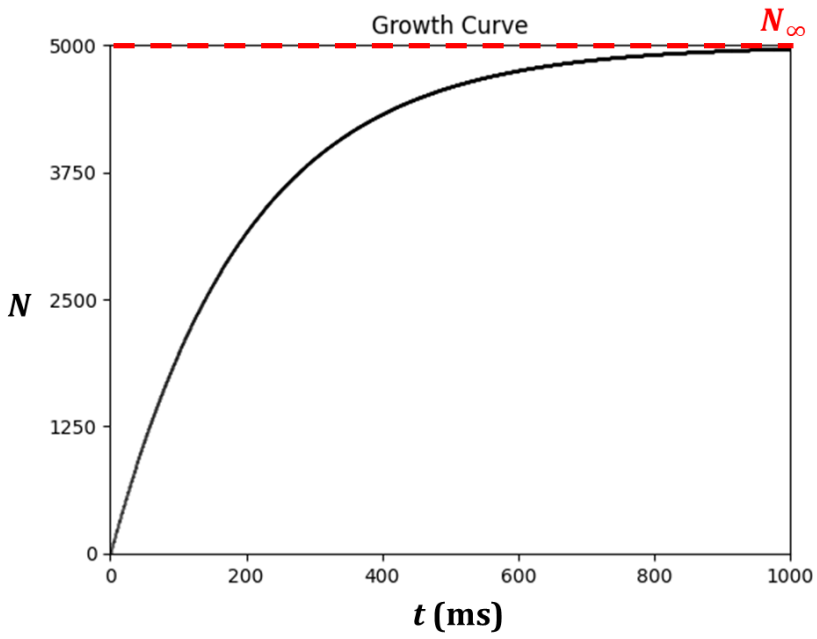

Figure 16. Example growth curve. The number of product nuclei, N, in a target being hit with a beam is increasing as more nuclear reactions occur. The product nuclei decay at a rate proportional the number remaining, causing the number of product nuclei to approach a maximum of N_∞.

So, the total number of product nuclei is given by

$$N = \frac{1}{\lambda}\frac{dN_c}{dt}\left(1 - e^{-\lambda t}\right). \tag{23}$$

As $t \to \infty$, the maximum number of product nuclei, N_∞, is

$$N_\infty = \frac{1}{\lambda}\frac{dN_c}{dt}, \tag{24}$$

so, the number of product nuclei can be written as

$$N = N_\infty\left(1 - e^{-\lambda t}\right). \tag{25}$$

Equation (25) can be expanded to give

$$\mathrm{N(t)} = N_\infty \left(1 - \left(1 - \lambda t + \frac{(\lambda t)^2}{2!} - \frac{(\lambda t)^3}{3!} + \frac{(\lambda t)^4}{4!} + \cdots\right)\right). \tag{26}$$

When $t \ll t_{1/2}$, then from Equation (15), $t\lambda \ll 1$, so

$$\mathrm{N(t)} \cong \mathrm{N}_\infty(\lambda t) = \frac{dN_c}{dt} t, \tag{27}$$

which is a linearly increasing function. TNSA ions and ICF neutrons will strike the nuclear target within ~100 ns, while the half-lives of the decays happen from 10 ms to 20 s, so when counting decays, it can be treated as though no decays occurred until after all the activation has occurred. For ^{8}Li, $t_{1/2} = 839.9$ ms $\gg 100$ ns, so in the experiment described in Section 0, the number of ^{8}Li product nuclei can be treated as though no decays occurred until well after all the product nuclei are created.

During a shot in the experiment, the detector did not detect only the desired ^{8}Li decays that were created on the nuclear target, but also detected background events from sources like cosmic rays, decays from any nearby materials, like steel, that may have been activated, or reactions with other isotopes, like ^{6}Li, in the target. So, the number of detected events, $N_d(t)$, after time, t, assuming a constant background rate, B, is

$$N_d(t) = \epsilon_d \left\{ Bt + \sum_{i=1}^{m} P_i (1 - e^{-\lambda_i t}) \right\}, \tag{28}$$

for m different decay reactions, each with an initial P_i number of radioactive nuclei, and detector efficiency, ϵ_d, which is the ratio of betas that were detected to number of betas emitted.

Chapter 3

OMEGA-EP TNSA EXPERIMENT

This chapter describes the OMEGA-EP TNSA experiment apparatus and the experimental procedure. Remember, in this experiment, shown in Figure 17, the OMEGA-EP laser is used to produce ^{8}Li. To do this, the sidelighter laser and backlighter laser are used to shoot a laser target to accelerate TNSA deuterons. A TPIE detector is used as a diagnostic to measure the incident deuteron energy spectrum, and the SLICS detector is used to measure the decays from the nuclear target placed just upstream from the SLICS.

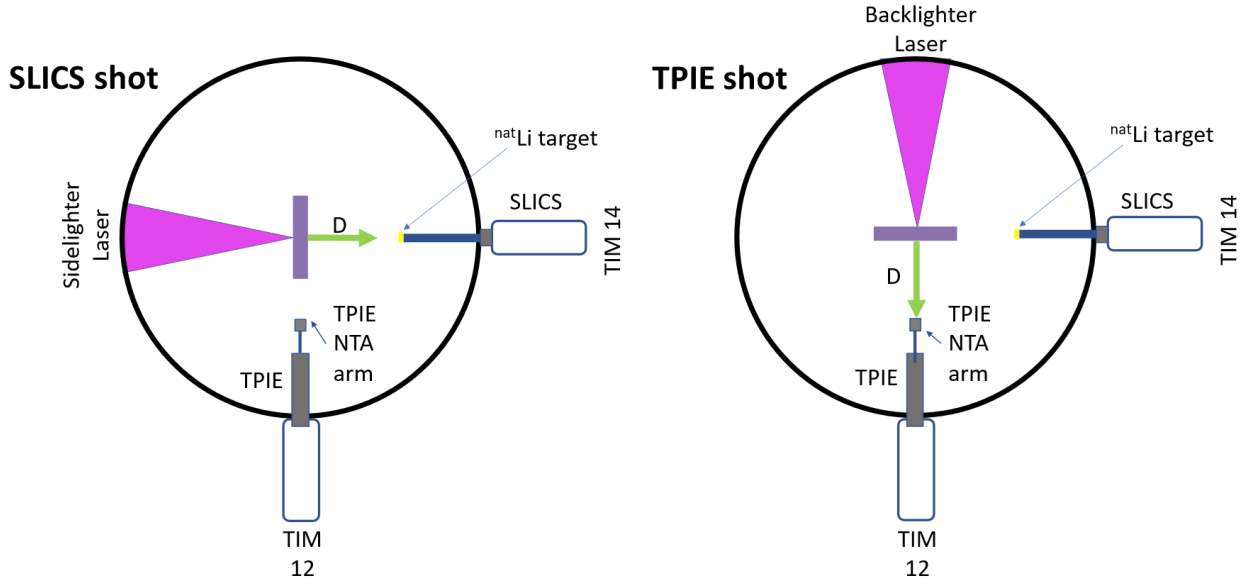

Figure 17. OMEGA-EP experiment. The OMEGA-EP made alternating shots between the sidelighter (left) and backlighter (right) lasers. The sidelighter laser struck a deuterated stainless-steel substrate causing TNSA deuterons to strike a thin lithium film on the end of the SLICS causing ^{7}Li(d,p)^{8}Li. The pTOF was used to estimate the deuteron energy spectrum. The backlighter laser was used to cause TNSA deuterons from a deuterated stainless-steel target to strike the TPIE to obtain the resulting energy spectrum.

3.1. OMEGA-EP Laser

The OMEGA-EP laser system, shown in Figure 18, at the Laboratory for Laser Energetics is comprised of four beams, two of which are short pulse beams: the sidelighter and backlighter

beams. These two beams are each able to deliver pulse lengths between ~0.7 and 100 ps with energies up to 500 J for the former pulse length, and 2000 J for the latter. The beams have a pointing accuracy of <75 μm and a timing accuracy of <25 ps. The lasers are directed into a target chamber, shown in Figure 19. The diagnostics and sidelighter and backlighter lasers are pointed at the center of the chamber where the laser target is held during the shot. Each beam has a shot rate of once per 90 min, so alternating beams allows shots to be taken every 45 min.

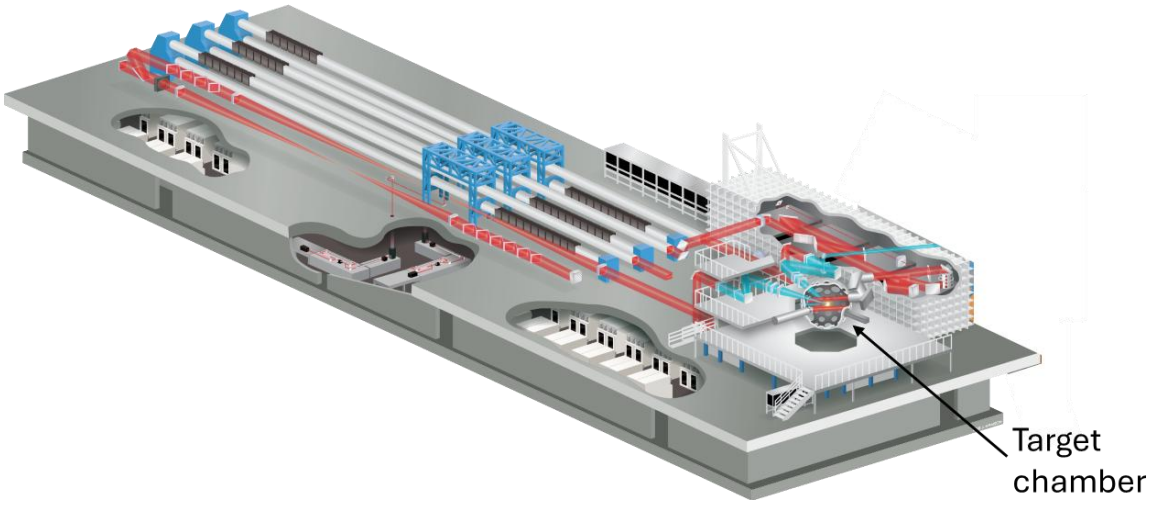

Figure 18. OMEGA-EP laser. OMEGA-EP consists of four laser beams that are directed into a target chamber. Two of the beams are short-pulse beams that can be used to perform TNSA experiments.

During a shot, the laser chamber is evacuated. Then for this experiment, a 10 ps square pulse duration, 100 μm focal spot diameter laser struck the laser target, with energies of about 135 J, 370 J, or 740 J depending on the shot.

3.2. Laser Target

The laser target flag, shown in Figure 20, was created using the procedure from Ref [7], except it was made of stainless-steel instead of titanium. Each 0.5 mm square 25 μm thick stainless-steel target was exposed to 400 °C, 950 Torr deuteron gas for 24 h causing the stainless-steel to absorb deuterons on the surface of the target. Initially, the laser targets had a thin, 1 μm thick, coating of titanium to create a deuterated titanium coating, but this was not present for later shots. The target flag was held by a stainless-steel flagpole that was

glued or crimped onto a standard LLE stalk, which allowed the target to be positioned in the OMEGA-EP chamber.

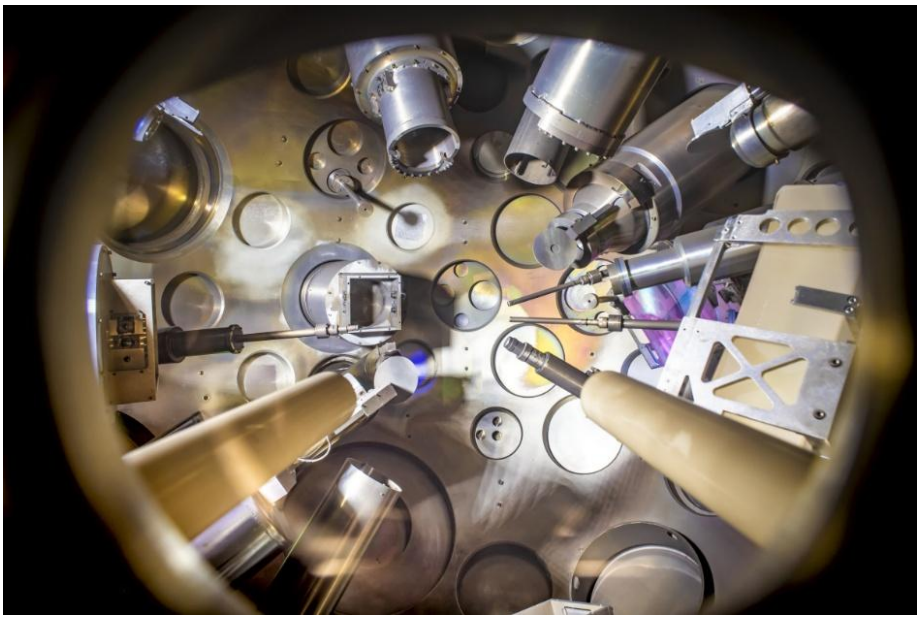

Figure 19. OMEGA-EP target chamber. The diagnostics and sidelighter and backlighter lasers are pointed towards the center of the chamber, where the laser target is held during a shot. Figure taken from Ref [25].

3.3. Thompson Parabola Ion Energy Analyzer

For alternating shots, TNSA accelerated deuterons from the backlighter laser entered the pinhole in the Thompson Parabola Ion Energy Analyzer (TPIE) detector. Figure 21 shows a charged particle passing through the magnetic and electric fields inside the TPIE detector. The ion was deflected vertically by a magnetic field, $\vec{B}$, where the force of the field, $\vec{F}_B$, is given by $\vec{F}_B = q\vec{v} \times \vec{B}$, where q is the charge and $\vec{v}$ is the velocity with magnitude $v = \sqrt{2T/m}$ where T is the kinetic energy and m is the mass of the incident particle. The particle was then deflected horizontally by the electric field, $\vec{E}$, where the force, $\vec{F}_E$, is given by $\vec{F}_E = q\vec{E}$. The deflected particle struck an image plate creating bands that corresponded to different charge to mass ratios of incident ions, allowing the particle to be identified based on using the horizontal deflection from the electric field along and the vertical deflection from the magnetic field. The density of the band at a given point corresponds to the number of ions with a particular energy. The image plate can be scanned to determine the energy

spectrum for each different ion incident on the TPIE according to the procedure described in Ref [7]. Figure 22 shows an example TPIE deuteron energy spectrum from multiple laser shots with laser energies about 370 J.

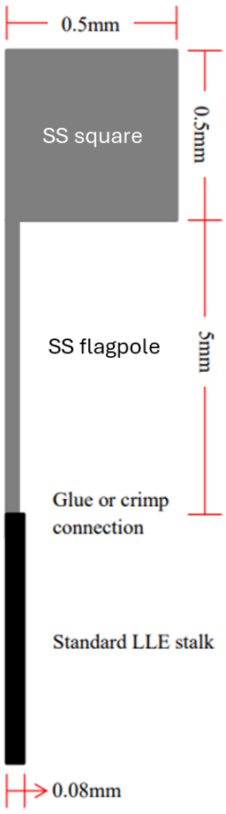

Figure 20. Stainless-steel laser target flag. The deuterated stainless-steel target was attached to a standard LLE stalk. The stalk allowed the target to be held and positioned inside the OMEGA-EP chamber. Figure adapted from Ref [7].

3.4. Lithium Films

Alternating shots with the TPIE, the laser target was rotated 90°, so the sidelighter laser, using ostensibly the same parameters as the backlighter shot, would accelerate the deuterons towards a thin lithium target placed on the front of the SLICS detector, shown in Figure 23 causing $^{7}Li(d,p)^{8}Li$.

3.4.1. Lithium Flim Target Fabrication

In order to make the target films [26], natural lithium pellets were heated in a stainless-steel boat at $\sim 10^{-6}$ torr causing Physical Vapor Deposition (PVD) to occur. The lithium was

deposited through a 16.76 mm diameter hole onto a 23.6 mm diameter, 25.4 μm thick stainless-steel substrate. The vacuum chamber was placed inside an argon glove bag as lithium is highly reactive and easily forms a wide variety of compounds. When exposed to humid air, the following reactions typically occur [27]:

$6\ Li(s) + N_2(g) \rightarrow 2\ Li_3N(s)$ (black)	$\Delta H(25°C) = -47.5$ kcal mol^{-1}
$2\ Li(s) + 2\ H_2O(g) \rightarrow 2\ LiOH(s)$ (black if anhydrous)$+ H_2(g)$	$\Delta H(25°C) = -48.7$ kcal mol^{-1}
$2\ LiOH(s)+ CO_2(g) \rightarrow Li_2CO_3(s)$ (white) $+ H_2O(g)$	
$LiOH(s) + H_2O(g) \rightarrow LiOH\cdot H2O(s)$ (white)	
$2\ Li(s) + O_2(g) \rightarrow Li_2O(s)$ (white)$+ ½\ O_2(g)$	$\Delta H(25°C) = -142.7$ kcal mol^{-1}
$4\ Li(s) + 3\ CO2(g) \rightarrow 2\ Li_2CO_3(s)$ (white)$+ C(s)$	$\Delta H(25°C) = -148.6$ kcal mol^{-1}

After deposition the Li targets were stored at atmosphere. Figure 24, shows the expected weight gain over time for lithium [27] stored in 27°C air of 50% humidity ending around 300% weight gain after 24 hours. It also shows the percent composition by weight of the film for multiple different compounds over the same 24-hour period, after which it was composed primarily of LiOH. After an even longer time, it becomes primarily Li_2CO_3.

3.4.2. Lithium Flim Thickness

After allowing the targets, shown in Figure 25, to become primarily Li_2CO_3, the target thicknesses were measured using SUNY Geneseo's 1.7 MeV Pelletron particle accelerator. A 1.51 MeV and a 1.31 MeV proton beam, normal to the lithium target, struck the 0.11 μm thick target causing $^{7}Li(p,\alpha)^{4}He$ reaction. The beam current was measured by placing a gold foil upstream from the lithium target and measuring the $^{197}Au(p,p)^{197}Au$ scattering reaction at 90°. for each run, the current was around 6-7 nA. The gold foil was then removed from the beam so it would strike the lithium target. The resulting $^{7}Li(p,\alpha)^{4}He$ alphas were measured with a 210 mm diameter silicon detector at a 166° angle with solid angle 0.0045 steradians. This repeated twice more at points across the target. The average thickness, shown in Table 1, was then calculated using the known $^{7}Li(p,\alpha)^{4}He$ cross-section. The primary uncertainty was from the spread of previously measured $^{7}Li(p,\alpha)^{4}He$ cross-sections that were used to calculate the thickness.

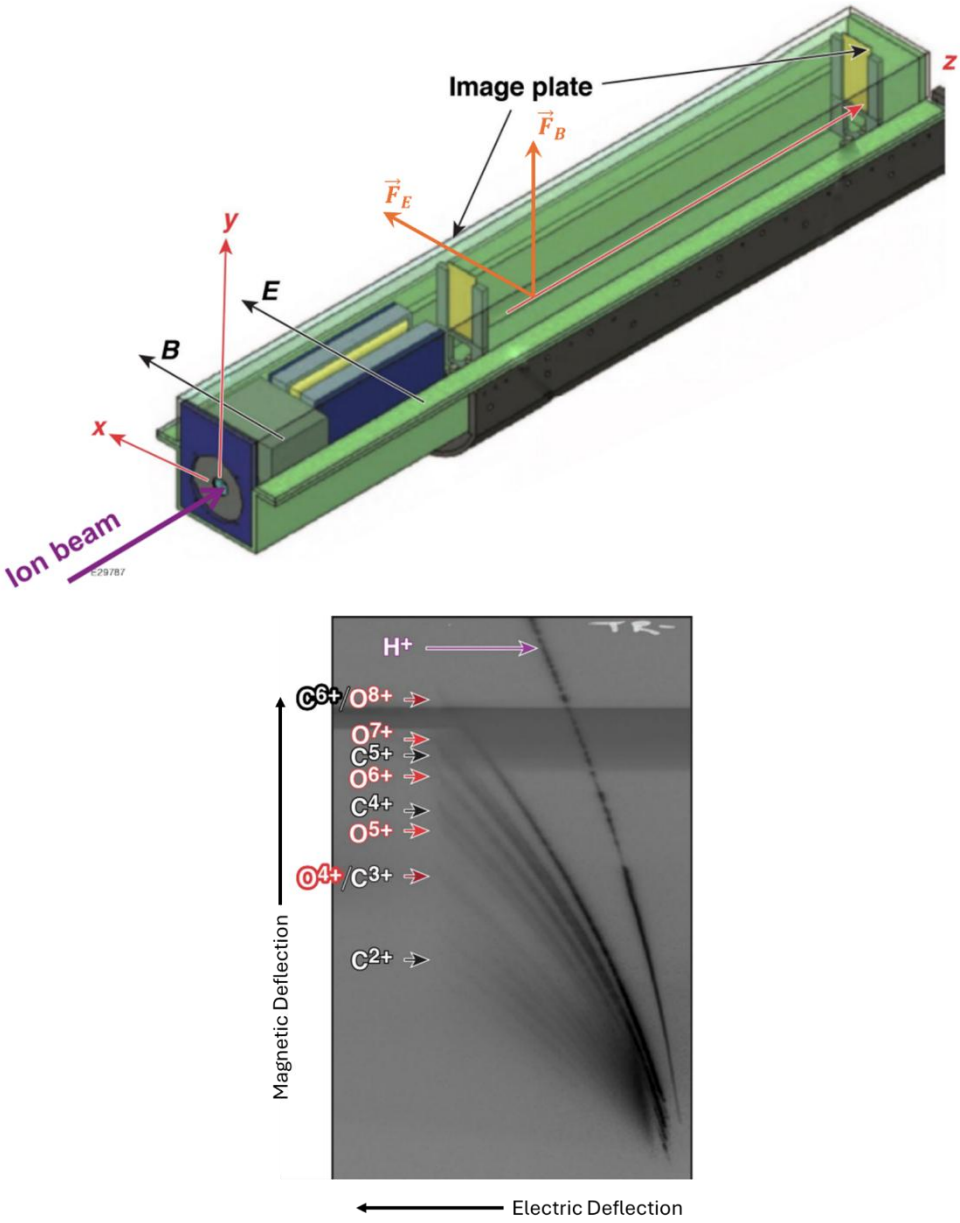

Figure 21. Thompson Parabola Ion Energy Analyzer (TPIE) Detector and image plate. A charged particle enters the TPIE detector (top) and is deflected vertically by a magnetic field depending on the charge, mass, and kinetic energy. Then it is deflected horizontally depending on charge and mass. This particle can be identified from the horizontal deflection from the electric field along with vertical deflection from the magnetic field. The charge then strikes an image plate (bottom) forming bands based on a charge to mass ratio. Positive ions with a higher charge to mass ratio are deflected more to the left, and those that have a higher kinetic energy are deflected more upward. Using this, the ions can be identified based on the bands that form laterally. The density at a given point on a band corresponds to the number of that ion with a particular energy. The image plate can be scanned to determine the energy spectrum for each ion incident on the TPIE.

3.5. Short-Lived Isotope Counting System

3.5.1. Particle Time-of-Flight Detector

The Particle Time-of-Flight (pTOF) detector, shown in Figure 26, was just upstream of the lithium target, and was used to measure the energy spectrum of the deuterons incident on the lithium target. After ~5-80 ns from the shot, the incident deuterons struck the pTOF detector, which is comprised of a 1mm EJ-212 scintillator coated first with a 200 nm layer of aluminum, to reduce light loss out of the scintillator, then a 200 nm layer of gold to reduce light leakage into the scintillator. The light from the scintillator travels down a fiberoptic cable to a Photek 240 photomultiplier tube.

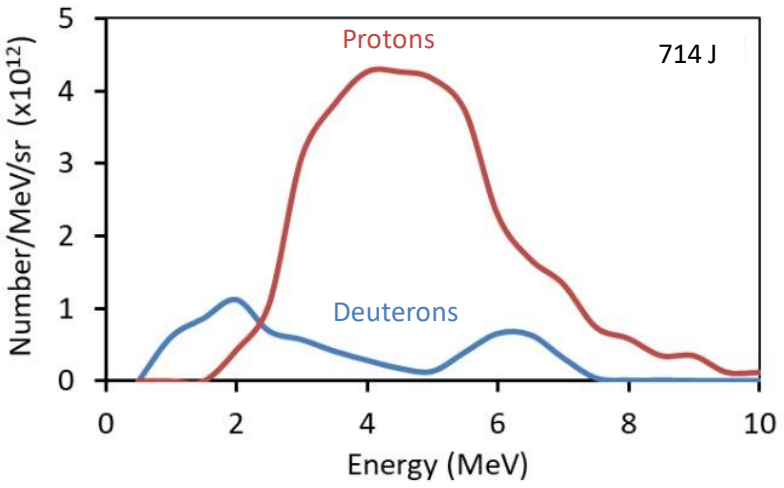

Figure 22. Plot of a TPIE energy spectrum. An example energy spectrum from an OMEGA-EP laser shot of 714 J. The deuterons and protons striking the target are not monoenergetic but have a spectrum of energies. The TPIE is able to separate the deuterons and protons, measuring their energies separately.

3.5.2. Short-Lived Isotope Counting System

The beta particles from the ^{8}Li pass into through the SLICS detector. Figure 27 shows a diagram of SLICS. The phoswich scintillator, shown in more detail in Figure 28, is comprised of a dE layer and an E layer. The dE layer is a 23.6 mm diameter, 1 mm thick EJ-200 plastic scintillator which has a decay time of 2.1 ns. The E layer is a 23.6 mm diameter, 18 mm thick EJ-240 plastic scintillator with a decay time of 285 ns. It is attached to the dE layer with EJ-500 optical epoxy. The light from the scintillators passes down a 25.4 mm diameter 308 mm long Schott F2 glass lightguide attached to the phoswich scintillator by EJ-500 optical epoxy.

The lightguide is attached to a 69.9 mm diameter, 6.4 mm thick Schott F2 glass window using vacuum baked EJ-500 epoxy. The epoxy to the glass window, along with spring clips, shown in Figure 29, near the scintillator end, are used to hold the lightguide in place, unlike previous iterations of SLICS, where the force from the o-ring held it in place. All the epoxy was baked at 45°C for 7.5 hours. The light travels through this into an ADIT 9807B photomultiplier (PMT) tube held at -2000 V.

Figure 23. Lithium target on SLICS. A lithium target was placed on the end of SLICS. Deuterons from the sidelighter laser struck the target causing $^{7}Li(d,p)^{8}Li$ reactions to occur.

3.5.3. TIM-Based Housing

The housing for the TIM-based SLCIS is comprised of three main components, shown in Figure 30: the bubble housing, the cable carrier assembly, and the exit bell. Due to the high voltages, the PMT and PMT base must be kept in atmosphere to prevent sparking. In order to achieve this, the bubble housing, shown in Figure 31, is designed to have an at atmosphere environment for the PMT, while the target chamber is evacuated. Additionally, the super high voltage cable also requires an airhose from the bubble to keep it at atmosphere. In order for SLICS to be inserted into the chamber and retracted without tangling the cables, the cable carrier assembly, shown in Figure 32, keeps the cables and airhose neat and prevents wear on the cables from repeated usage. The cables exit the TIM through a standard TIM exit bell, shown in Figure 33, that contains the feedthroughs for the signal and high voltage cable, along with the pTOF fiberoptic cable. Figure 34 shows the housing inside a TIM, where it can extend 1.676 m from its fully retracted to fully extended position.

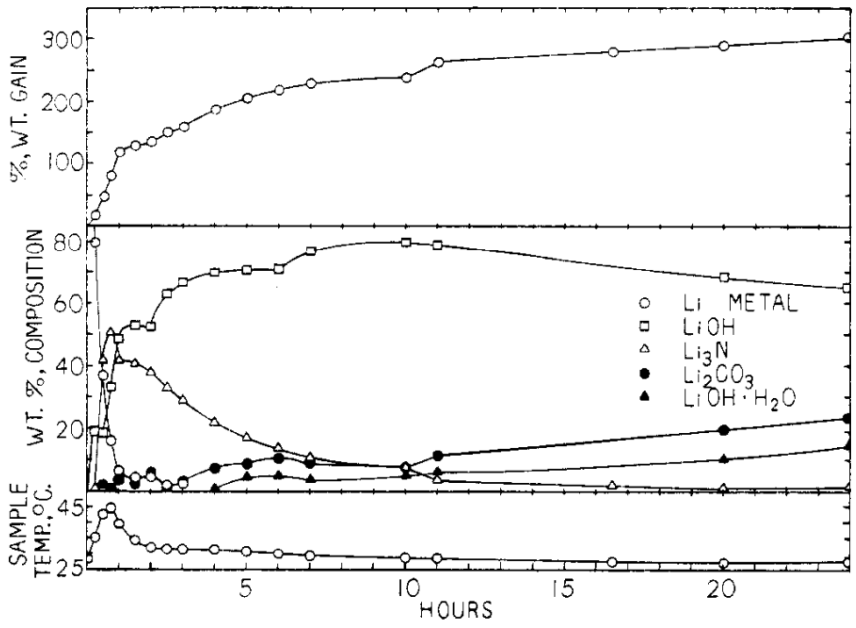

Figure 24. Compounds of Li over time in 27°C air of 50% humidity. The top graph shows the weight gain over time for lithium, ending around 300% weight gain after 24 hours. The middle plot shows the wt.% composition of the film for multiple different compounds over the same 24-hour period, after which it was composed primarily of LiOH. The bottom plot shows the temperature of the sample over time due to the reactions. Figure taken from Ref [27].

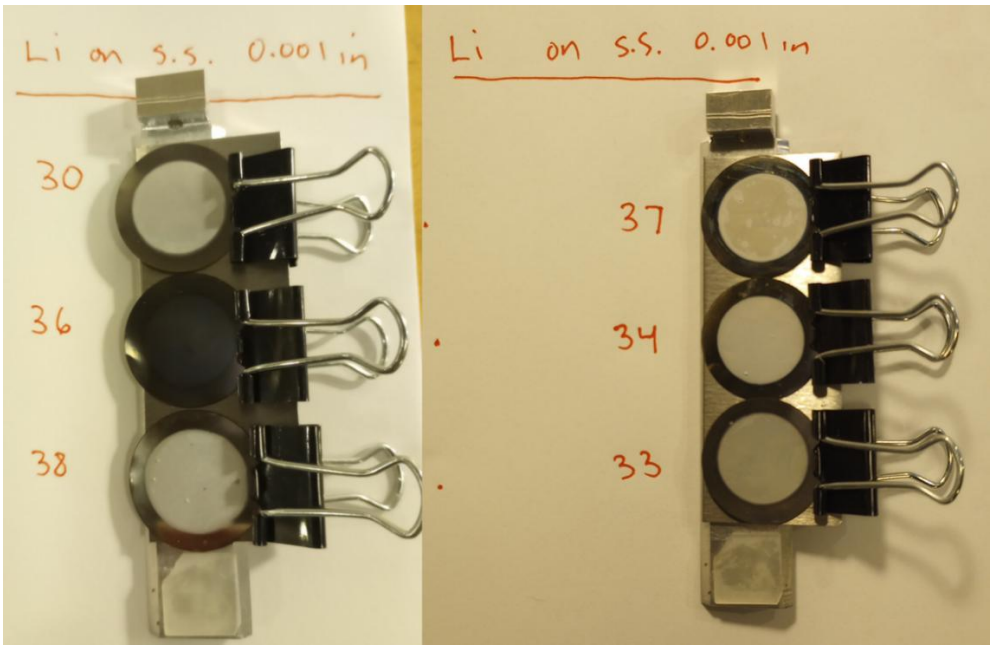

Figure 25. Lithium targets. Oxidized lithium targets of varying thicknesses were measured using the Pelletron particle accelerator at SUNY Geneseo.

Table 1. Thickness of ^{8}Li targets, as measured using the SUNY Geneseo Pelletron particle accelerator.

Target No.	Thickness (μm)
30	1.5
33	0.53
34	1.1
37	0.34
38	3.5

3.5.4. Positioning and Alignment

Using TIM 12, the SLICS detector was inserted into the OMEGA-EP target chamber. In TIM 12, SLICS clears the fixed diagnostics, shown in Figure 35, along with both sidelighter and backlighter lasers. TIM-based SLICS can also be inserted into TIM 14, where it will clear the fixed diagnostics and the sidelighter laser, but must be retracted during backlighter shots. When inserted, the SLICS was initially 35 cm from the laser target, but it was subsequently moved back to 51 cm, then 100 cm, after debris from the laser target scoured the lithium from the nuclear target. In order to line up SLICS with the laser target, a pointer assembly, shown in Figure 36, was mounted to the front of the detector. The distance from the nuclear target to the TCC at the end of the pointer assembly is 23 cm.

3.5.5. Electronics

When a shot happened, the PMT was disconnected from the High Voltage and digitizer electronics by an isolation relay circuit, to protect them from the EMP from the shot. Figure 37 shows the timeline after a shot. It was only after ~1 ms that the post shot environment was quiet enough to measure the ^{8}Li decays, at which point a Raspberry Pi 4, connected to the OMEGA timing system, then closed the Oono F-1049 relay and connected the PMT and the digitizer. Then, the light from the scintillators was converted to a voltage pulse by the PMT, like the example shown in Figure 38, except much noisier. The signal pulse from the phototube traveled to the CAEN N6730SB digitizer, where it was sampled every 2 ns for 800 ns starting 80 ns before the pulse. The samples were read into the Atomic Pi, via a USB 2.0, which saved the digitized pulse waveform for analysis. Pulses were collected for ~30 s. If the

rate of data acquisition was too high, the digitizer would save more pulses than the Atomic Pi could read out, and if the rate was high enough, the RAM on the digitizer would fill up causing gaps in the data collected, as saved pulses were overwritten in the digitizer.

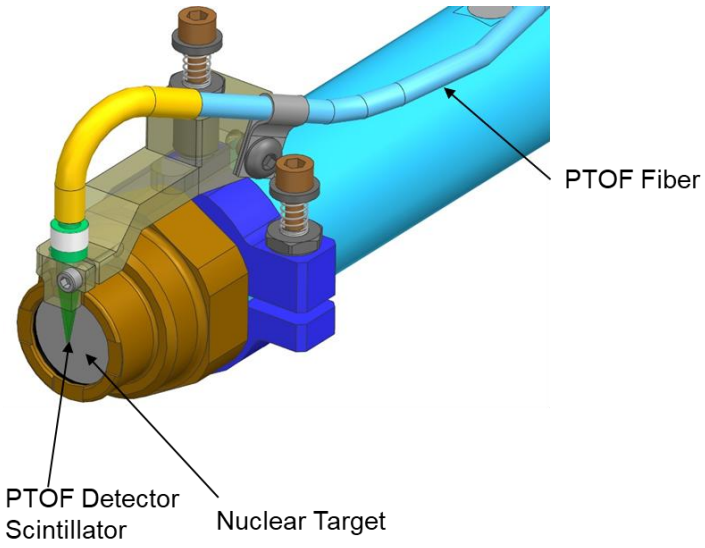

Figure 26. PTOF schematic diagram. The pTOF is placed on the end of the SLICS detector. It is comprised of an EJ-212 scintillator coated in aluminum then gold. The scintillation light travels down a fiberoptic cable into a Photek 240 photomultiplier.

Each pulse that is saved is a superposition of two pulses, shown in Figure 38, a fast pulse from the dE layer and a slow decaying pulse from the E layer. This signal was separated back into the two components, by dividing the pulse into two sections. The first gate, from 0 ns to 70 ns, contains primarily the short pulse, and the gate from 70 ns to 100 ns containing primarily the long pulse. The area under the peak for each gate was proportional to the energy lost in the corresponding scintillator layer.

3.5.6. Efficiency Calibration

Plotting the energy lost in each layer in a 2D histogram, like the one shown in Figure 39, allowed good beta events to be identified based on the region of the plot. In order to calibrate this, a GEANT 4 simulation of a ^{207}Bi source on the face of the detector was compared to events detected by SLICS. A box was drawn where most of the good beta decays from ^{8}Li fall. The efficiency was obtained by determine the number of ^{207}Bi events from the simulation that fell within the box, then using the SLICS ^{207}Bi calibration to match the energy scales.

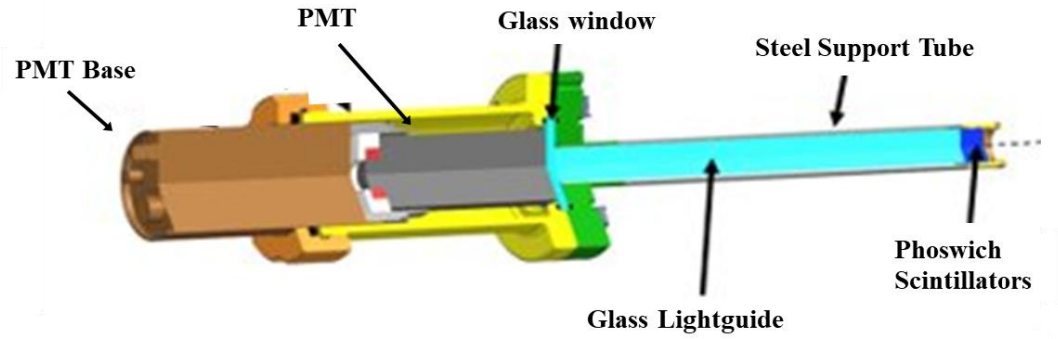

Figure 27. Prototype SLICS schematic design. The light from the scintillators travels through a 25.4 mm diameter 308 mm long Schott F2 glass lightguide, attached to a 69.9 mm diameter, 6.4 mm thick Schott F2 glass window using vacuum baked EJ-500 Epoxy. The light travels through this into a photomultiplier tube, where the light is converted into a digital signal.

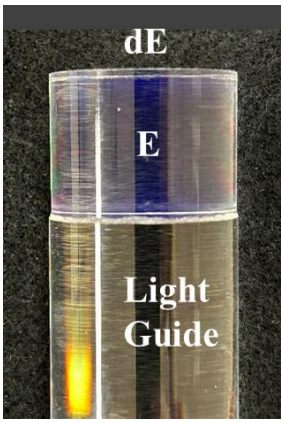

Figure 28. Phoswich scintillator closeup. The phoswich scintillator is comprised of a dE layer and an E layer. The dE layer is a 23.6 mm diameter, 1 mm thick EJ-200 plastic scintillator which has a decay time of 2.1 ns. The E layer is a 23.6 mm diameter, 18 mm thick EJ-240 plastic scintillator with a decay time of 285 ns. It is attached to a 25.4 mm diameter 308 mm long Schott F2 glass lightguide. Between each layer is EJ-500 optical epoxy.

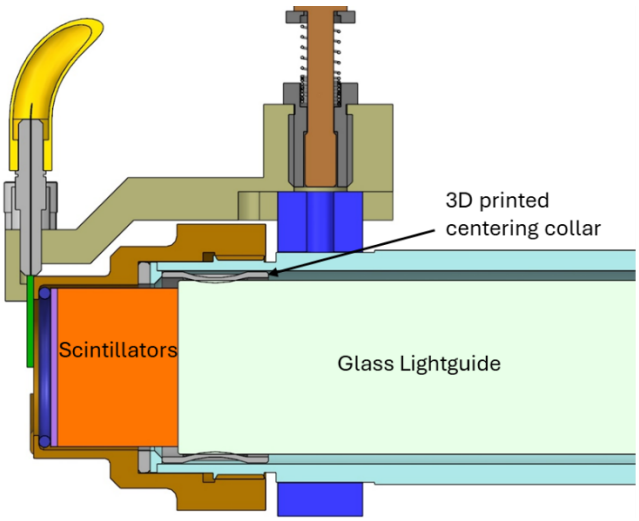

Figure 29. Lightguide support drawing. Two spring clips support one end of the lightguide while the other side is epoxied to a glass window in order to hold the lightguide in place.

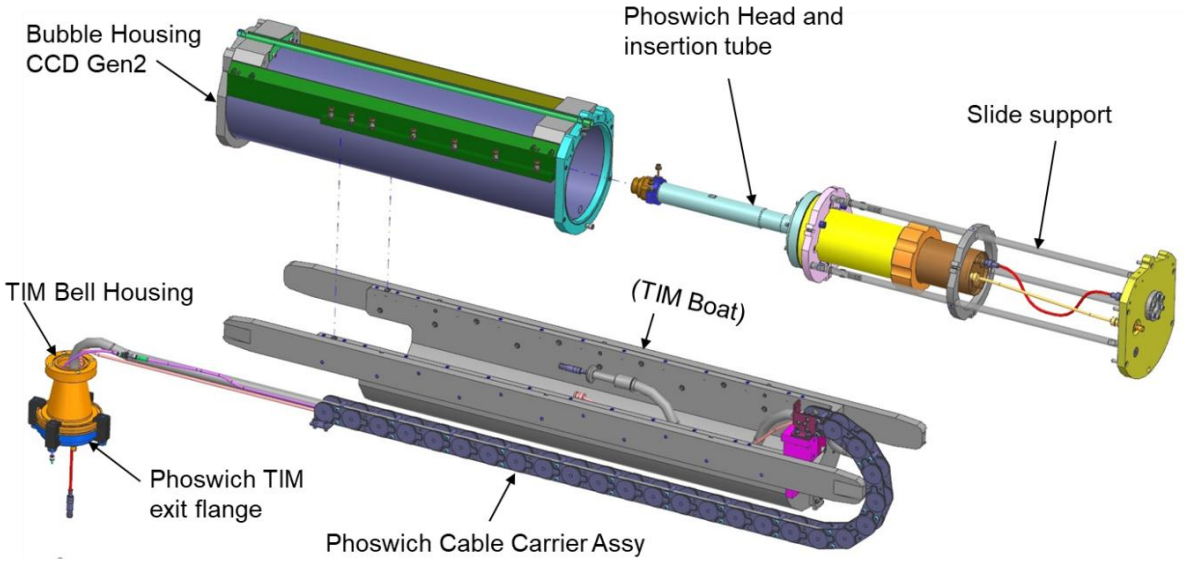

Figure 30. TIM-based SLICS exploded drawing. The TIM-based SLICS is housed inside a bubble, with the signal cables and airhose contained in a cable carrier assembly, exiting via a standard TIM exit bell.

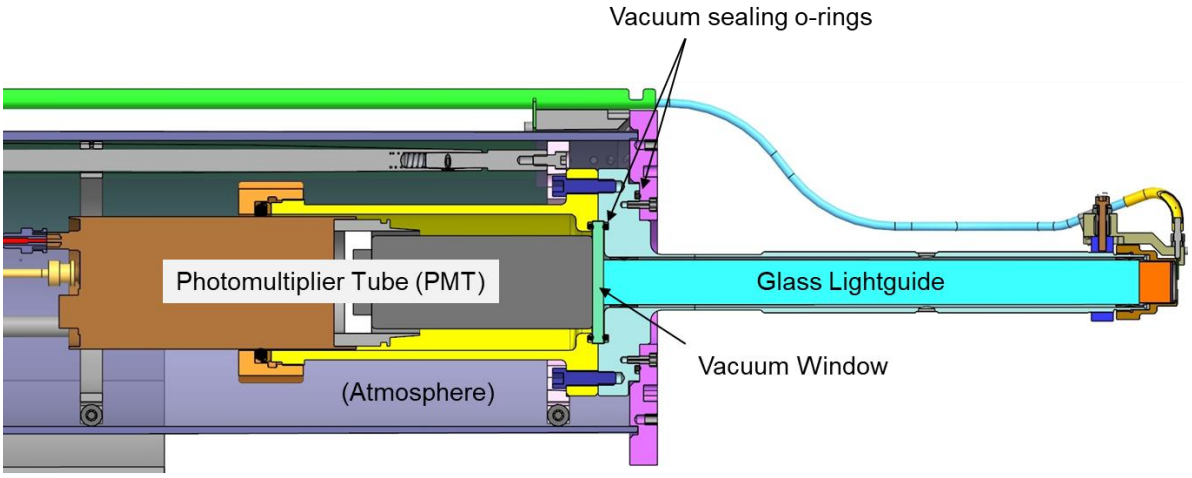

Figure 31. Air bubble drawing. The PMT and PMT base are kept at atmosphere in the bubble to prevent sparking from the high voltage.

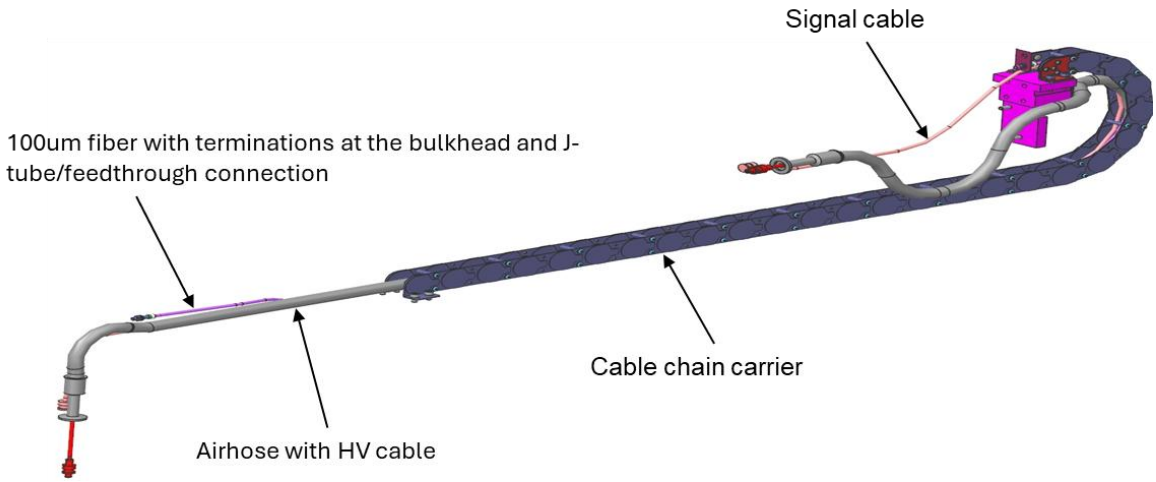

Figure 32. Cable chain drawing. The cable chain allows the SLICS to be extended and retracted from the TIM without the cables becoming tangled.

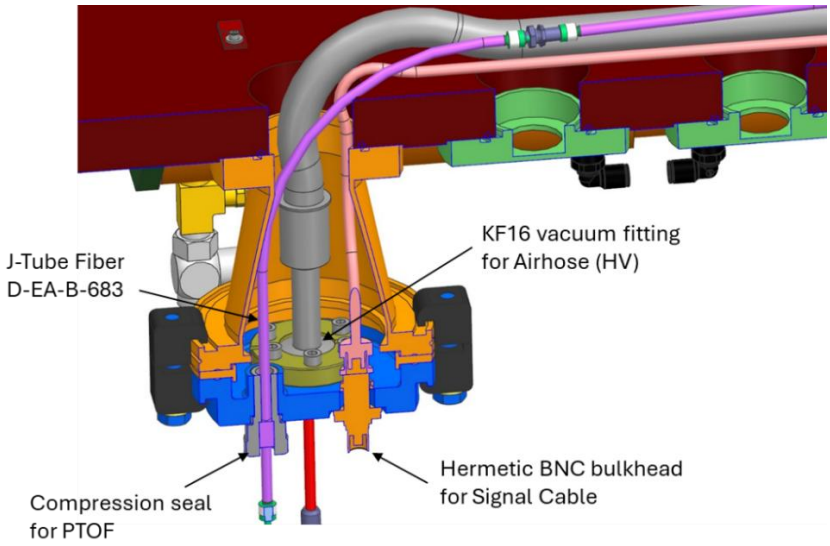

Figure 33. Exit bell drawing. The SLICS utilizes a standard TIM exit bell containing the feedthroughs for the high voltage and signal cables for the SLICS, along with the one for the fiberoptic cable from the pTOF.

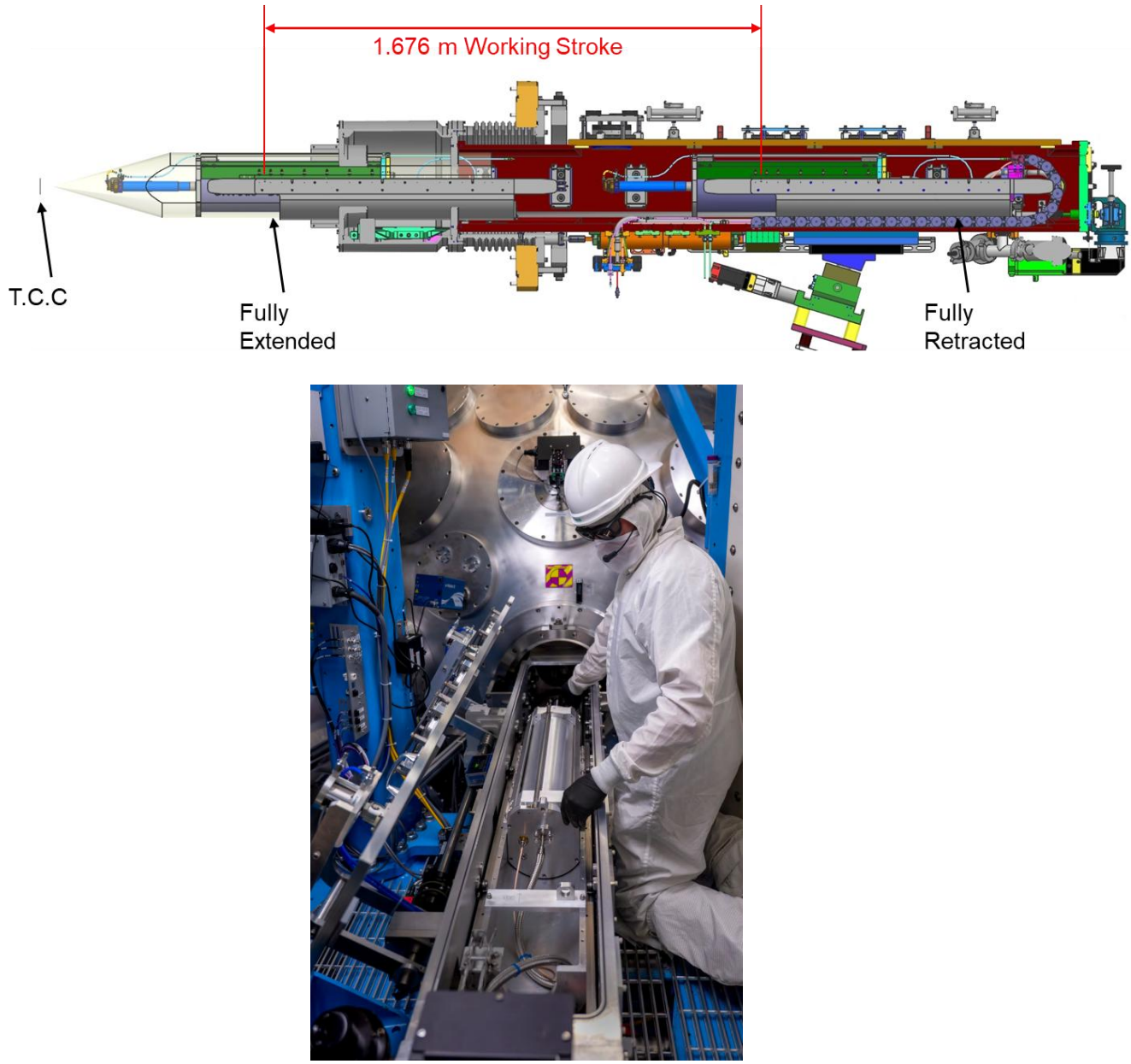

Figure 34. SLICS inside TIM. The assembly allows the SLICS to be extended up to 1.676 m (top). The SLICS inside the TIM while in the retracted position (bottom).

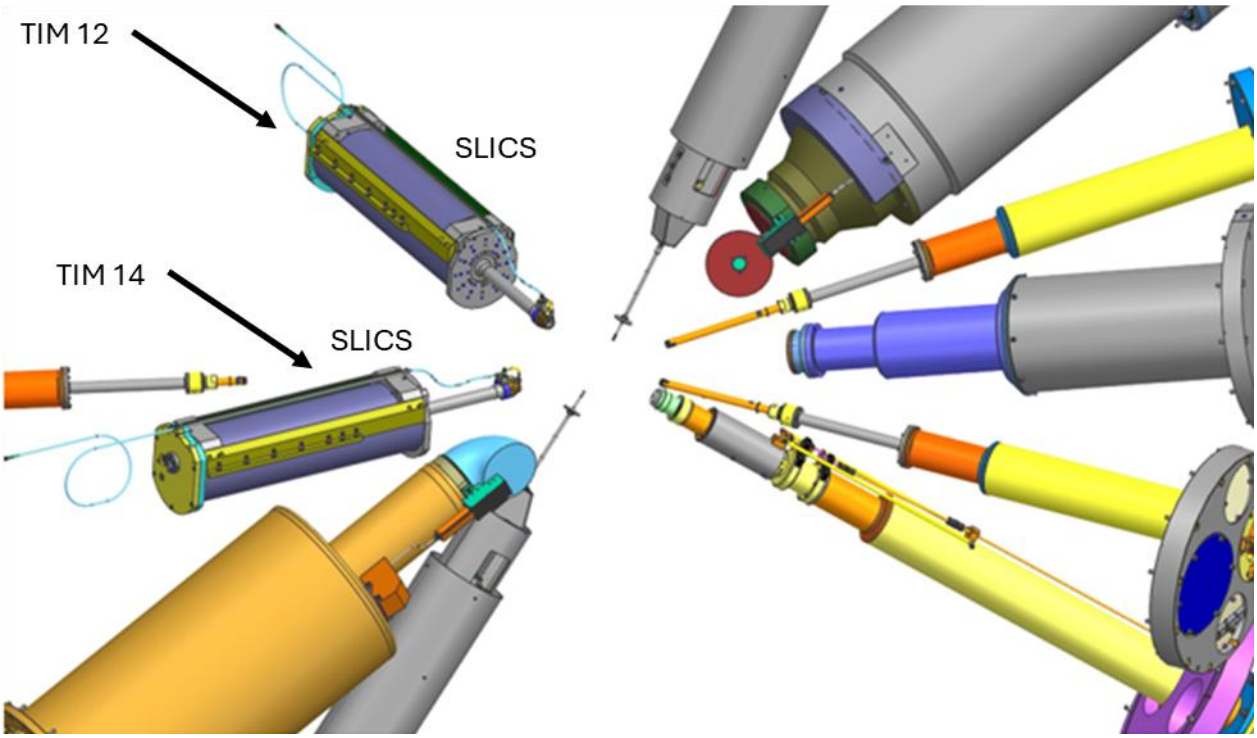

Figure 35. SLICS clearance in OMEGA-EP. When fully inserted into the OMEGA-EP chamber, the TIM-based SLICS will clear all the other fixed diagnostics in TIM 12 and TIM 14.

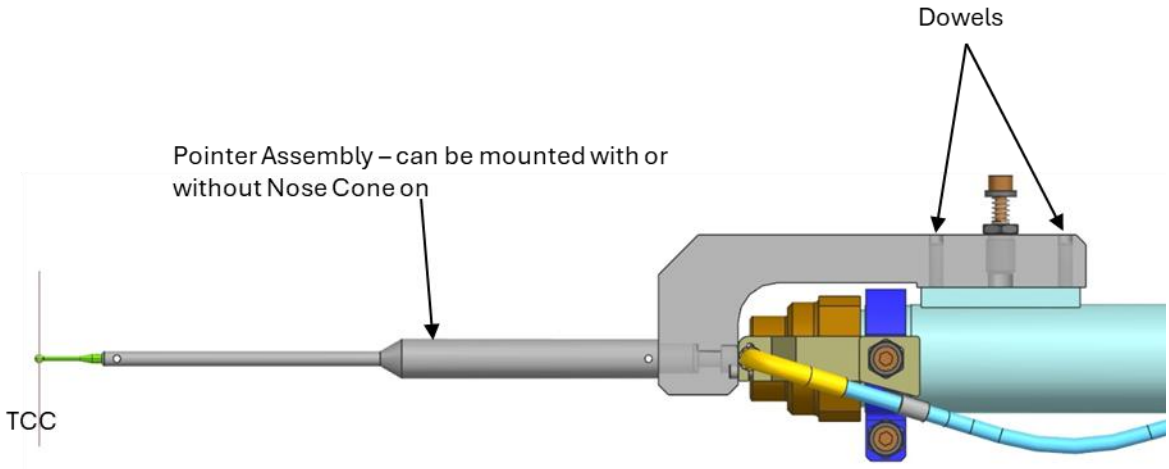

Figure 36. Pointer assembly. The pointer assembly can be mounted to the front of SLICS to line up SLICS with the laser target. The TCC on the end of the pointer is 23 cm from the nuclear target.

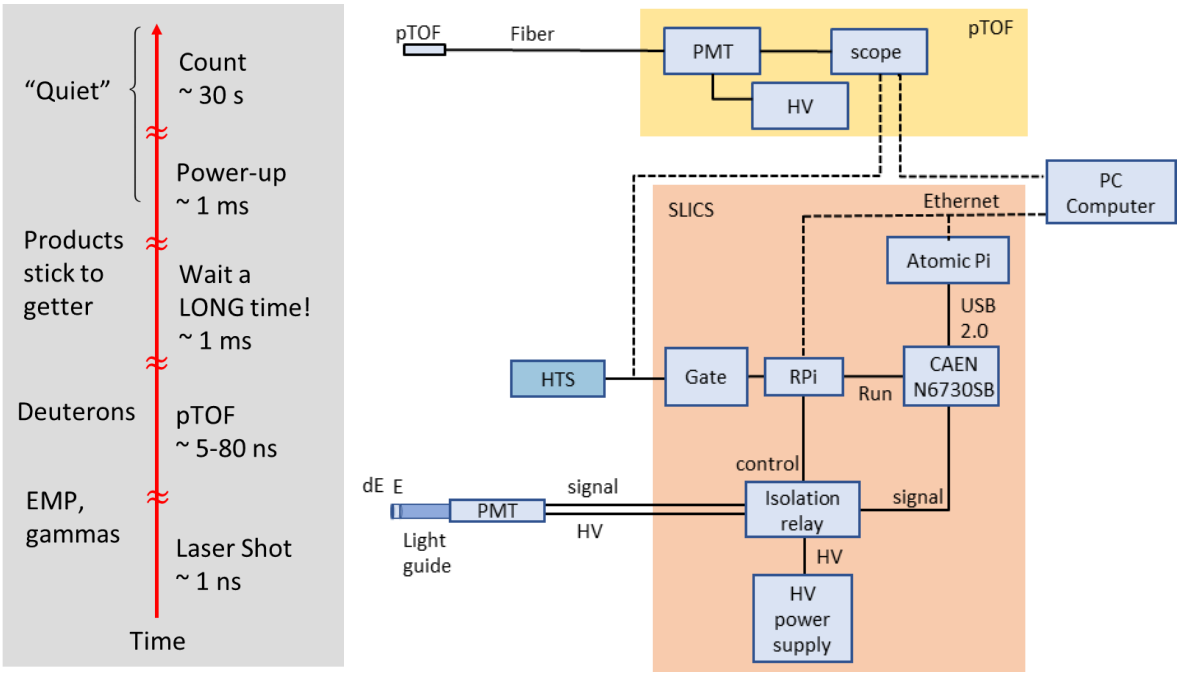

Figure 37. Shot timeline (left) and electronics (right). After ~1 ns from the shot, an EMP and gammas, moving at the speed of light reach the SLICS detector. After ~5-80 ns, the deuterons that were accelerated reach the pTOF. After ~1 ms, the Raspberry Pi sends a signal to close the isolation relay to the SLICS and turn on the PMT. The detector then counts decays for ~30 s in the relatively quiet environment after the shot. The signal pulses from the now connected PMT traveled to the CAEN N6730SB digitizer where each pulse was sampled every 2 ns for an 800 ns window around the pulse. This pulse was then saved for analysis by the Atomic Pi.

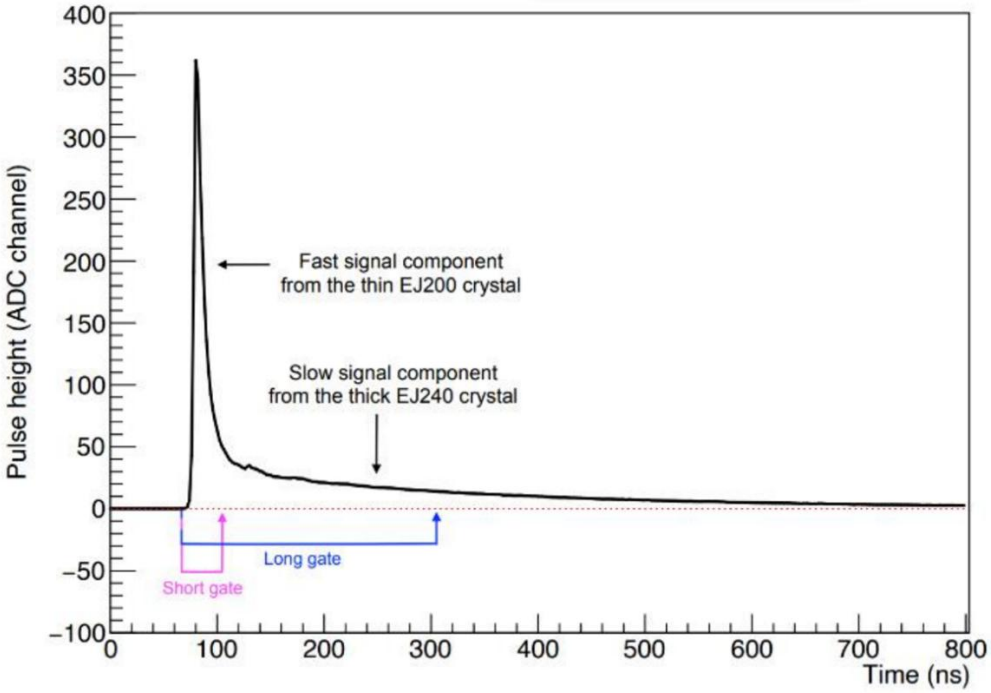

Figure 38. PMT signal pulse. The output signal from the PMT was a superposition of the light from the dE and E layers. The short gate (pink) was primarily from the dE layer, while the long gate (blue) was primarily from the E layer, with the area corresponding to each proportional to the energy the particle lost in each layer. Figure taken from Ref [13].

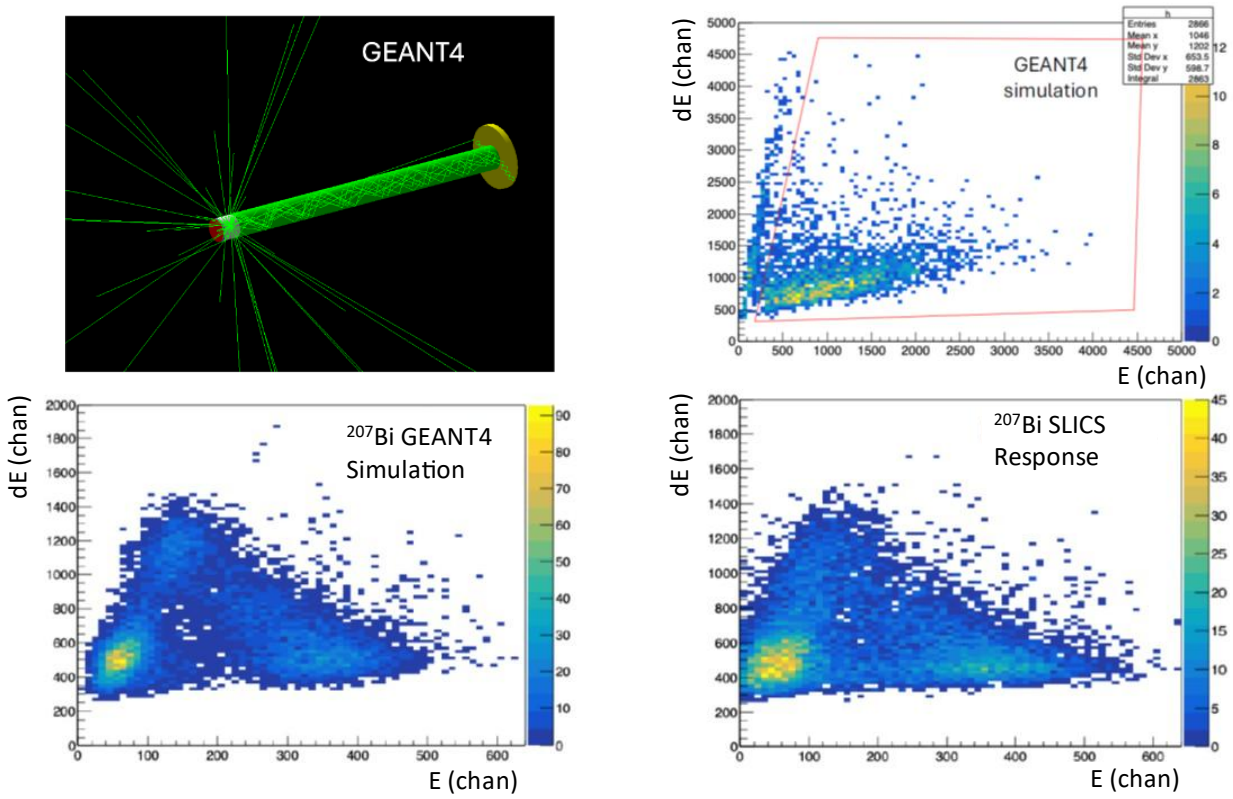

Figure 39. ^{207}Bi calibration plots. GEANT4 was used to simulate (top left) a ^{207}Bi plot (bottom left). The efficiency was determined by comparing the ratio of ^{207}Bi decays inside the box outlined in red to the total number of simulated decays. This was compared with the ratio obtained by counting the decays of a ^{207}Bi source using SLICS (bottom) that fell within the outlined red box to the total number of decays that occurred. This was used to calibrate efficiency so simulations of ^{8}Li decays could be compared to the SLICS measurements. Figure adapted from Ref [13].

Chapter 4

RESULTS AND ANALYSIS

4.1. Decay and Growth Curves

In this experiment, OMEGA-EP accelerated TNSA deuterons towards a lithium target, forming ^{8}Li. The resulting beta decay from the ^{8}Li were detected by the phoswich scintillator in SLICS. The light from the scintillators was digitized and separated back into the components from the dE and E scintillators. Two 1D histograms, shown in Figure 40, were created showing the number of events that lost different amounts of energy in the dE and E scintillators. Each event was then plotted on a 2D histogram, showing the amount of energy lost in each scintillator for that event. Different types of particles lost different amounts of energy in each scintillator, appearing in different regions of the 2D histogram. Some particles, like protons and alphas, lost primarily all their energy in the dE layer, before making it through to the E layer. Other particles that rarely interact, like gammas, will primarily interact with, if at all, the much thicker E layer. A box, shown in Figure 40, was drawn around where most of the good beta decay events occurred. The number of total decays was calibrated using a GEANT-4 simulation, like the one shown in Figure 39, by determining the fraction of the total ^{8}Li decays that fell within the box, which was the efficiency. The position of the box from the simulation was calibrated to measured histogram using a ^{207}Bi source, which has a distinctive monoenergetic peak.

The events inside the box were histograms as a function of time, binned in intervals of 1 ms. The resulting histogram, like the one shown in Figure 40, forms a decay curve, like the one in Equation (14). Integrating this curve gives the growth curve, like the one in Equation (28). The decay histogram is not integrated from $t = 0$, since the SLICS detector did not start collecting data right away. A small delay is introduced, so that the integration starts at the maximum decay rate, at which point the SLICS has started data acquisition for at least a full bin. To account for this, Equation (14) is used to find the number of activated nuclei at $t = 0$. The plot of the integrated decay histogram can be fitted using MINUIT [28], with a growth curve with a linear background, the primary decay from ^{8}Li, and a secondary decay source.

The half-life for ^{8}Li was fixed, but the other half-life and the coefficients were allowed to vary. The residual is the difference between the fitted curve and the measured number, with a better fit having a smaller residual. Figure 41 shows growth curves at three different energies, 139 J, 370 J, and 724 J, showing the lithium decays, a secondary activation, and a linear background, along with the corresponding residuals. Table 2 shows the number of ^{8}Li decays detected by SLICS, along with the secondary decaying isotope and background for each shot, determined using Equation (28).

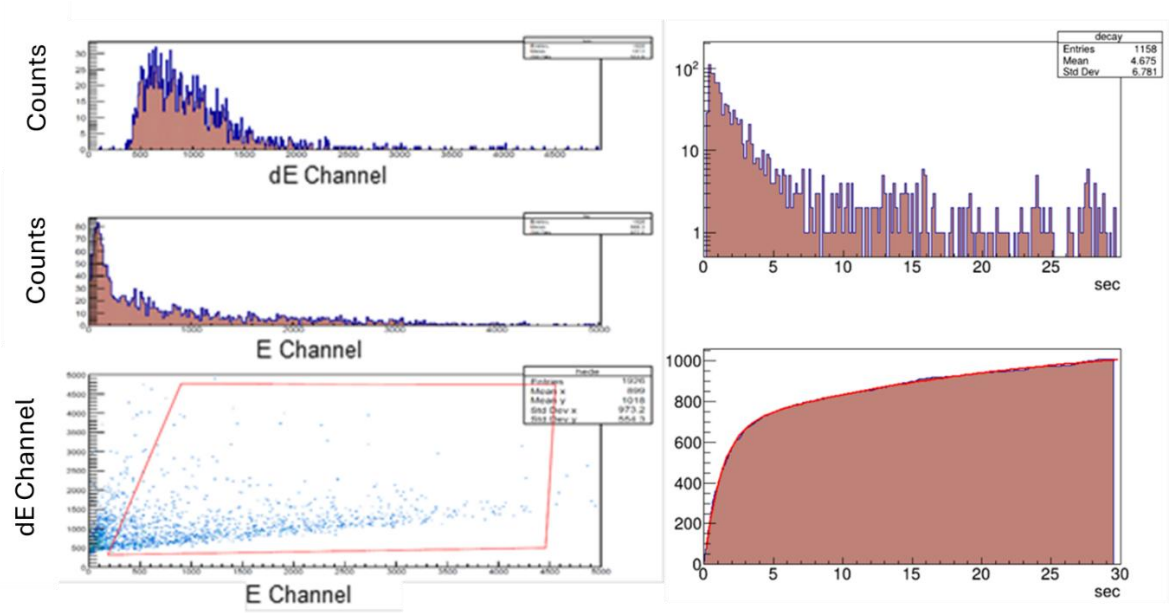

Figure 40. Histograms. A 1D histogram can be plotted with the energy lost in the dE (top left) and E (middle left) layers. A 2D histogram (bottom left) can also be made using the energy lost in each scintillator. Good ^{8}Li decays will fall in the box outlined in red. Each event in the box is plotted on a time histogram with 1 ms bins to obtain the decay curve (top right), which can be integrated to get the integrated decay curve (bottom right). This can be fitted (red curve) with two growth curves and a linear background, to obtain the number of ^{8}Li decays

4.2. ^{8}Li yield

While doing multiple shots on the same target positioned 35 cm from the laser target, only the initial shot produced ^{8}Li. Upon inspection, it was discovered that debris from the laser target had scoured the lithium from the target substrate, shown in Figure 42, so there was no lithium remaining for subsequent shots. A new target was then moved back to 51 cm,

where the target was no longer scoured, but was still damaged and pockmarked with debris, so the target was moved back to 100 cm from the laser target.

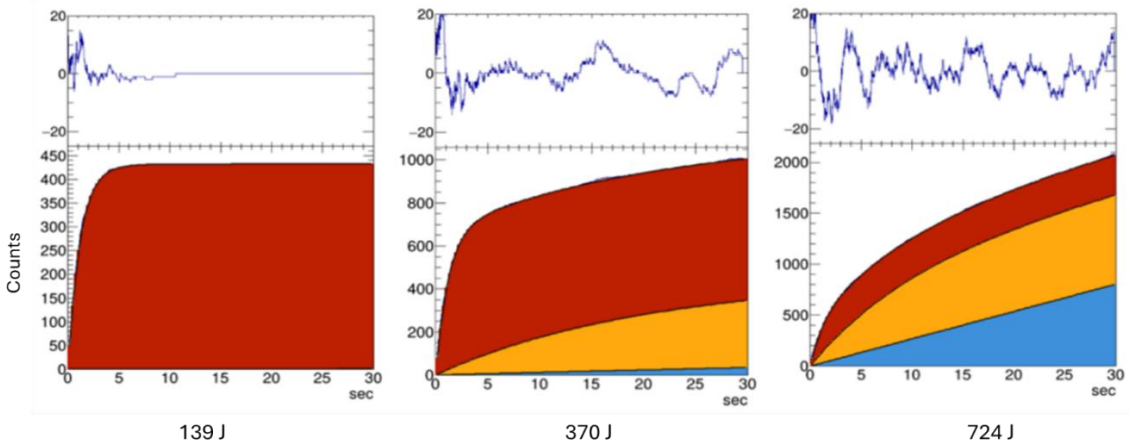

Figure 41. Growth curves of different energies. Growth curves (bottom) for OMEGA-EP shots 43438, at 139 J (left), 43424, at 370 J (center), and 43441, at 724 J (right). The red area indicates ^{8}Li decays, the blue indicates the background, and the yellow indicates the decays from an unknown isotope. The residuals (top) show the difference between the data and the fitted curve.

Table 2. Results of the fits used to determine the number of ^{8}Li created in each laser shot.

Shot	Laser Energy (J)	Integration Delay (s)	^{8}Li number detected ($t_{1/2} = 838.79$ ms)	Other number detected	Other λ (s^{-1})	Other Half-life (s)	Background number detected (s^{-1})
43417	364.0	2.00	505.8 ± 4.4	481.9 ± 98.4	0.071 ± 0.013	9.8 ± 1.8	8.4 ± 2.4
43424	370.0	0.50	659.2 ± 3.7	385.6 ± 134.7	0.056 ± 0.015	12.4 ± 3.3	1.1 ± 2.6
43426	3650	1.60	338.6 ± 4.0	292.1 ± 213.2	0.053 ± 0.030	13.1 ± 7.4	1.4 ± 4.2
43430	382.8	0.25	175.8 ± 2.3	112.2 ± 13.7	0.102 ± 0.015	6.8 ± 0.1	3.7 ± 0.4
43438	139.0	0.09	431.6 ± 0.001	0 ± 0.1			0
43441	724.0	0.12	392.4 ± 4.8	918.6 ± 31.0	0.104 ± 0.004	6.7 ± 0.3	26.8 ± 1.0

From the shots where the target was not destroyed, the counts obtained from the box on the 2D histogram were divided by the efficiency determined using the GEANT simulation to determine the total number of ^{8}Li that was created. The ^{8}Li/Li yield measurements, shown in Figure 43, were compared to predictions using the TPIE deuteron spectrum with the

previously measured ^{7}Li(d,p)^{8}Li cross sections at these different energies. Shots using laser targets with Ti coatings were excluded due to concerns of contamination with water, as they were much older than the stainless-steel laser targets.

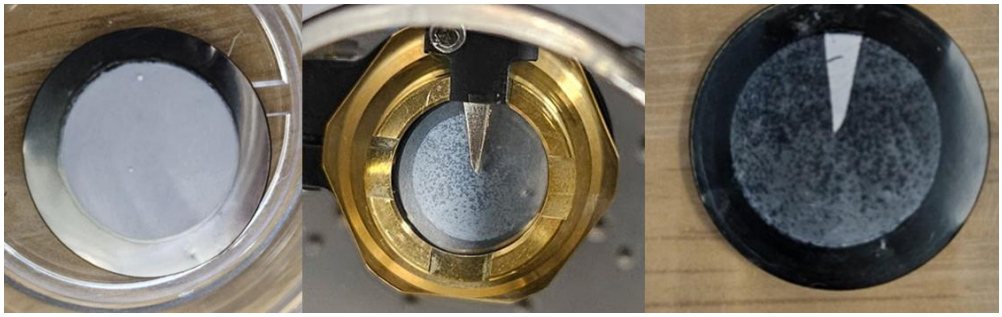

Figure 42. Scoured lithium films. Nuclear Target 34 before shot #43423 (left) was placed 35 cm from the laser target. Target 34 after shot #43423 still on the SLICS (center) had most of the lithium was scoured from the target, in addition to the gold coating on the TPIE detector. A small slice (right) of lithium remained on the target from the shadow of the TPIE detector.

The energy spectrum from the TPIE can be used to obtain a time-of-flight spectrum since the time-of-flight, t, for a particle is $t = d/\sqrt{2T/m}$, where d is the distance traveled, T is the kinetic energy of the particle, and m is the mass of the particle. Figure 43 shows the time-of-flight spectrum from the pTOF compared to the time-of-flight spectrum obtained from the TPIE energy spectrum from shots at similar energies. The pTOF time-of-flight spectrum is close to the deuteron time-of-flight spectrum plus the proton time-of-flight spectrum obtained from the TPIE energy spectrums.

The measured yield had systematic uncertainty from the efficiency, and statistical uncertainty. There was additional systematic uncertainty from variations in target thickness, and the spread of previously measured ^{7}Li(p,α)^{4}He cross-sections that were used to calculate the target thickness. The predictions based on the TPIE energy spectrum had uncertainty due to the range in previously measured ^{7}Li(d,p)^{8}Li and due to uncertainty in the deuteron beam energy spectrum.

There was general agreement between the measured and predicted yields for both ~360 J and ~720 J, suggesting that the TIM-based SLICS is capable of measuring light ion reaction cross-sections in TNSA experiments. Additionally, the agreement between the TPIE and

pTOF energy spectrums indicates that these measurements could be carried out only using SLICS, without alternating shots between SLICS and TPIE. This would especially be the case if only the desired incident ions were accelerated towards the nuclear target.

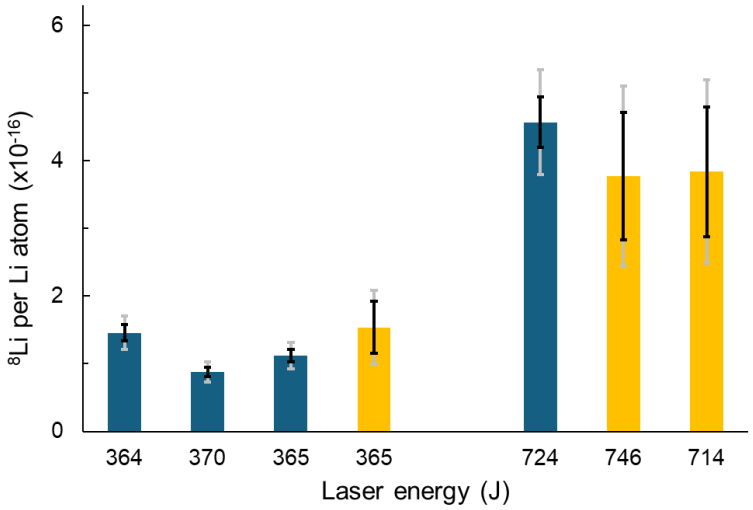

Figure 43. ^{8}Li/Li atom yield histogram. The number of ^{8}Li created per Li atom in the nuclear target for ~370 J and ~730 J as measured by the SLICS (blue) and the predicted yield based off the scaled TPIE deuteron energy spectrum (yellow) The error bars for SLICS represent the efficiency uncertainty (8%) and the counting uncertainty (1%) inherent to SLICS (black) and the additional uncertainty due to variations in target thickness and the previous measurements of ^{7}Li(p,α)^{4}He in addition to the inherent uncertainty (grey). The error bars for the predictions based on the TPIE measurements is due to the range in previously measured ^{7}Li(d,p)^{8}Li cross-sections (black), and the added deuteron beam uncertainty (grey). Figure taken from Ref [13].

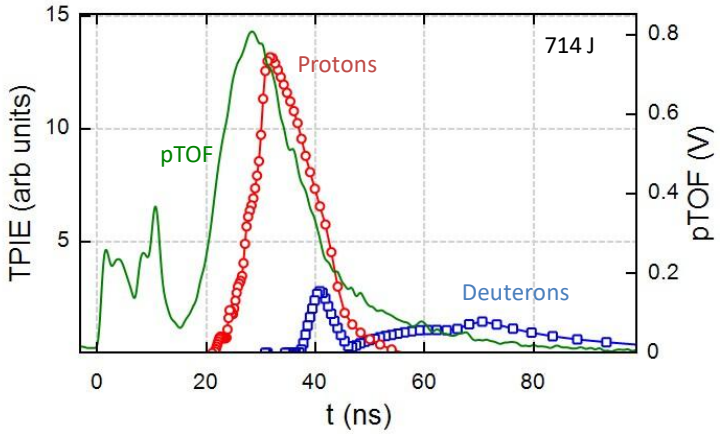

Figure 44. PTOF time-of-flight spectrum. The energy spectrum obtained from the pTOF (green) is compared to one obtained from the TPIE proton (red) and deuteron (blue) spectrums.

Chapter 5

FUTURE PLANS

The TIM-based SLICS is currently considered a standard diagnostic for the OMEGA laser system. Two future experiments are currently being planned to measure the reactions ^{6}Li(t,p)^{8}Li and ^{7}Li(t,a)^{6}He using SLICS. Due to being tritium reactions, the experiments would be joint shots using the OMEGA-EP lasers to accelerate TNSA tritons towards a lithium target in the OMEGA-60 target chamber, which can handle tritium. For the former reaction, special nuclear targets using enriched ^{6}Li targets will be used due to the low abundance of ^{6}Li in natural lithium.

Due to tritium being radioactive, the current method of creating deuterated flag laser targets will not work with tritium. In order to do these tritium experiments, new laser targets were designed to contain the tritium. The targets consist of a small cylinder with cryogenic tritium on one end. An experiment was initially planned to measure ^{7}Li(t,a)^{6}He reaction but was postponed due to the OMEGA-60 chamber being unable to use both the TIM-based SLICS and the TPIE simultaneously.

Additionally, TIM-based SLICS is a prototype detector for the proposed NSF-OPAL laser [14], which will be designed for high shot-rate experiments. The high shot rate will allow for more shots to be performed each day for an experiment, which will improve the result statistics, as with a monoenergetic beam of incident ions, one shot will give one cross-section, but with an energy spectrum, the cross-sections must be deconvoluted from the energy spectrum requiring multiple shots for a single cross-section. Additionally, if provided with a tritium capable chamber, this will eliminate the need for a joint shot for tritium using the OMEGA-EP lasers to produce a triton beam in the OMEGA-60 chamber which is able to handle tritium. One of the proposed flagship NSF-OPAL experiments is measuring the ^{7}Li(t,γ)^{10}Be and ^{7}Li(t,n)^{9}Be reactions using the SLICS detector.

Appendix A

TIMING AND ANALYSIS CODE

Below is the C code, SLICS.c, for the RaspberryPi that controlled the isolation relays for the PMT and digitizer.

```
#include <stdlib.h>
#include <stdio.h>
#include <pigpio.h>
// to compile:  gcc SLICS.c -o SLICS -l pigpio

int main(int argc, char *argv[])
{

float duration;
int secs, microsecs;

// Read in the commend line arguments
if(argc!=2) {
  printf("Usage: SLICS <duration>\n");
  printf("   duration = length of time to enable digitizers (s)\n");
  exit(0);
   }
duration = atof(argv[1]);
printf("Enabling digitizers for %f seconds.\n",duration);
secs = duration;
microsecs = (int)((duration - secs)*1000000);
printf("  %d secs  %d microsecs\n",secs, microsecs);

// Initialize the pigpio library
if (gpioInitialise() < 0)
  {
  fprintf(stderr, "pigpio initialisation failed\n");
  return 1;
  }
/* Set GPIO modes */
gpioSetMode(2, PI_OUTPUT);    // enable CAEN digitizer when high
gpioSetMode(19, PI_OUTPUT);   // HV+ground relay
gpioSetMode(26, PI_OUTPUT);   // signal+ground relay
gpioSetMode(13, PI_INPUT);    // laser trigger input

// turn everything off
gpioWrite(2,0);
gpioWrite(19,0);  // HV+ground relay
gpioWrite(26,0);  // signal+ground relay

// wait for pulse from laser control
while(gpioRead(13) == 0){   }

// Delay turning on HV?
// gpioSleep(PI_TIME_RELATIVE, 0,5000);  // secs + microsecs

// turn on relays
gpioWrite(19,1);  // HV+ground relay
gpioWrite(26,1);   // signal+ground relay

// start digitizers
// Delay to wait for relays to stop bouncing
gpioSleep(PI_TIME_RELATIVE, 0 , 100000);
gpioWrite(2,1);     // enable CAEN

// Wait while data are collected
printf("Run Started\n");
gpioSleep(PI_TIME_RELATIVE,     secs,microsecs);          //     seconds+
microseconds
// End of experiment -- turn everything off, disagble digitizer
gpioWrite(2,0); // stop CAEN digitizer
gpioWrite(19,0);  // HV+ground relay
gpioWrite(26,0);  // signal+ground relay
printf("Run Ended HV off\n");
gpioTerminate();
return 0;
}
```

Below is the ROOT 29 C++ macro code, analyze.c, for the analyzer used to plot the energy histograms and determine ^{8}Li counts from the resulting growth curves.

```
// # analyze.C
// analyze data file containing wave data from CAEN N6730
//

// (c) 2021 Houghton College
//  Author: M. Yuly
// Created: 2021/10/26


#include <iostream>

// The following define must be set to the actual number of connected boards
#define MAXNB   1
// NB: the following define MUST specify the ACTUAL max allowed number of board's channels
// it is needed for consistency inside the CAENDigitizer's functions used to allocate the memory
#define MaxNChannels 8

// The following define MUST specify the number of bits used for the energy calculation
#define MAXNBITS 16

// Number of samples of waveform to save 2ns/chan
#define WAVECHAN 400

// Baseline channels
#define BASELINE_START 0
#define BASELINE_END  35

// Short gate channels
#define SHORT_START  35
#define SHORT_END  50

// long gate channels
#define LONG_START 50
#define LONG_END 250

// number of bins for the decay and growth histogram
#define NUM_TIME_BINS 3000

// Maximum number of events allowed
#define MAX_EVENTS 10000000

//
// Gloval variables
//
uint16_t b,ch,ev, wsize;
int Eshort, Elong;
ULong64_t timestamp,extended,clocks;
int16_t www[WAVECHAN];

TCutG *cutg=new TCutG("mycut",5);
TString *run_name = new TString("unknown");

float duration;
float tdiv;
bool incut[MAX_EVENTS];

// ++++++++++++++++++++++++++++++++++++++++++++++++++++++
// saved WAVE version
//
// Load the TFile to create a TTree that will not disappear
// Parameters: name of root data file (*.root) and acquisition duration (sec)
// Usage:  load("Run_001",35)
// ++++++++++++++++++++++++++++++++++++++++++++++++++++++
void gload(TString fname="test",float fduration=300) {

//Create the root file
TString *root_name = new TString(fname);
root_name->Append(".root");
```

```
*run_name=root_name->Data();

// save duration for use in time histograms
duration = fduration;

printf("Opening run run file: %s\n", root_name->Data());


TFile *f=new TFile(root_name->Data());
TTree *t1=(TTree*)f->Get("t1");

t1->SetBranchAddress("b",&b);
t1->SetBranchAddress("ch",&ch);
t1->SetBranchAddress("ev",&ev);
t1->SetBranchAddress("size",&wsize);

t1->SetBranchAddress("timestamp",&timestamp);
t1->SetBranchAddress("Eshort",&Eshort);
t1->SetBranchAddress("Elong",&Elong);
t1->SetBranchAddress("extended",&extended);
t1->SetBranchAddress("clocks",&clocks);
t1->SetBranchAddress("WaveLine",www);

}


// ++++++++++++++++++++++++++++++++++++++++++++++++++++
// NO WAVE saved version
//
// Load the TFile to create a TTree that will not disappear
// Parameters: name of root data file (*.root) and acquisition duration
(sec)
// Usage:  load("Run_001",35)
// ++++++++++++++++++++++++++++++++++++++++++++++++++++
void qload(TString fname="test",float fduration=300) {

//Create the root file
TString *root_name = new TString(fname);
root_name->Append(".root");
```

```
*run_name=root_name->Data();

// save duration for use in time histograms
duration = fduration;

printf("Opening run run file: %s\n", root_name->Data());


TFile *f=new TFile(root_name->Data());
TTree *t1=(TTree*)f->Get("t1");

t1->SetBranchAddress("b",&b);
t1->SetBranchAddress("ch",&ch);
t1->SetBranchAddress("ev",&ev);
t1->SetBranchAddress("size",&wsize);

t1->SetBranchAddress("timestamp",&timestamp);
t1->SetBranchAddress("Eshort",&Eshort);
t1->SetBranchAddress("Elong",&Elong);
t1->SetBranchAddress("extended",&extended);
t1->SetBranchAddress("clocks",&clocks);
//t1->SetBranchAddress("WaveLine",www);

}
// ++++++++++++++++++++++++++++++++++++++++++++++++++++
// Set up the graphical cuts
// ++++++++++++++++++++++++++++++++++++++++++++++++++++
void set_cuts() {

cutg->SetVarX("Elong");
cutg->SetVarY("Eshort");
cutg->SetLineColor(2);
cutg->SetPoint(0,895.453,1481.86);
cutg->SetPoint(1,4741.93,9569.71);
cutg->SetPoint(2,58010.4,9890.27);
cutg->SetPoint(3,53475.8,3133.95);
cutg->SetPoint(4,895.453,1481.86);

}
```

```
// ++++++++++++++++++++++++++++++++++++++++++++++++++++
// Set up the canvas and histograms for Energy
// ++++++++++++++++++++++++++++++++++++++++++++++++++++
void make_Ehists() {

//Create energy histograms and display
printf("Creating Energy Histograms.\n");

TCanvas *c1 = new TCanvas("c1",run_name->Data(),1000,10,700,800);

TPad *pad1 = new TPad("pad1", "pad1",0.03,0.75,0.98,0.98);
TPad *pad2 = new TPad("pad2", "pad2",0.03,0.45,0.98,0.68);
TPad *pad3 = new TPad("pad3", "pad3",0.03,0.02,0.98,0.43);

TH1F *hde=new TH1F("hde", "",1000,0,10000);
TH1F *he=new TH1F("he", "",1000,0,20000);
TH2F *hede=new TH2F("hede", "",500,0,60000,500,0,10000);

pad1->Draw();
pad2->Draw();
pad3->Draw();

pad1->cd();
pad1->GetFrame()->SetFillColor(18);
hde->SetFillColor(45);
hde->SetLabelSize(0.06,"XY");
hde->Draw();

pad2->cd();
pad2->GetFrame()->SetFillColor(18);
he->SetFillColor(45);
he->SetLabelSize(0.06,"XY");
he->Draw();

pad3->cd();
hede->SetFillColor(45);
hede->SetLabelSize(0.03,"XY");
hede->Draw();

c1->Update();
c1->Draw();
}


// ++++++++++++++++++++++++++++++++++++++++++++++++++++
// Set up the canvas and histograms for time
// ++++++++++++++++++++++++++++++++++++++++++++++++++++
void make_thists() {

TString unit;

//Create time histograms and display
printf("Creating Time Histograms.\n");

TCanvas *c3 = new TCanvas("c3",run_name->Data(),1000,10,700,840);

TPad *pad1 = new TPad("pad1", "pad1",0.03,0.53,0.98,0.98);
TPad *pad2 = new TPad("pad2", "pad2",0.03,0.05,0.98,0.50);

if (duration>300)  {
   unit = "min";
   tdiv=60;
}
else {
   unit = "sec";
   tdiv=1;
}

TH1D *growth=new TH1D("growth",
"",NUM_TIME_BINS,0,duration/tdiv);
TH1D *decay=new TH1D("decay", "",NUM_TIME_BINS,0,duration/tdiv);

pad1->SetBottomMargin(0.15);
pad2->SetBottomMargin(0.15) ;
pad1->Draw();
pad2->Draw();
```

```
pad1->cd();
pad1->GetFrame()->SetFillColor(18);
decay->SetFillColor(45);
decay->SetLabelSize(0.06,"XY");
decay->GetXaxis()->SetTitle(unit.Data());
decay->GetXaxis()->SetTitleSize(0.06);
decay->Draw();

pad2->cd();
pad2->GetFrame()->SetFillColor(18);
growth->SetFillColor(45);
growth->SetLabelSize(0.06,"XY");
growth->GetXaxis()->SetTitle(unit.Data());
growth->GetXaxis()->SetTitleSize(0.06);
growth->Draw();

c3->Update();
c3->Draw();
}

// ++++++++++++++++++++++++++++++++++++++++++++++++++++++++
// Set up canvas and histgram for waves
// ++++++++++++++++++++++++++++++++++++++++++++++++++++++++
void make_whists() {

//Create wave  histograms and display
printf("Creating  Wave Histograms.\n");

TCanvas *c2 = new TCanvas("c2","CAEN wave",1000,10,700,510);
TH1F *h2=new TH1F("h2","",400,0,798);
h2->GetXaxis()->SetTitle("Time (ns)");
h2->Draw();

}

// ++++++++++++++++++++++++++++++++++++++++++++++++++++++++
// Fill a quick Histogram of Elong and Eshort integrals from the CAEN
// Does NOT require saved WAVES
// ++++++++++++++++++++++++++++++++++++++++++++++++++++++++
void qhist() {

make_Ehists();
TTree *t1=(TTree*)gDirectory->Get("t1");
TCanvas *c1=(TCanvas*)gROOT->GetListOfCanvases()->FindObject("c1");
TH1F *hde=(TH1F*)gDirectory->Get("hde");
TH1F *he=(TH1F*)gDirectory->Get("he");
TH2F *hede=(TH2F*)gDirectory->Get("hede");

int nentries = (Int_t)t1->GetEntries();
printf("nentries=%d\n",nentries);

for (int i=0;i<nentries;i++) {

  t1->GetEntry(i);

  hde->Fill(Eshort);
  he->Fill((Elong-Eshort));
  hede->Fill((Elong-Eshort),Eshort);

  // test the cut
  if (cutg->IsInside((Elong-Eshort),Eshort)) incut[i]=true; else incut[i]=false;
}
cutg->Draw();
cutg->Print();
c1->Update();
c1->Draw();
}

// ++++++++++++++++++++++++++++++++++++++++++++++++++++++++
// Fill energy histograms based on simple short and long gate integration
// Requires saved WAVES
// ++++++++++++++++++++++++++++++++++++++++++++++++++++++++
void ghist() {

int n_baseline_chan, baseline_sum ;
```

```
float baseline;

int short_int, long_int;

make_Ehists();
TTree *t1=(TTree*)gDirectory->Get("t1");
TCanvas *c1=(TCanvas*)gROOT->GetListOfCanvases()->FindObject("c1");
TH1F *hde=(TH1F*)gDirectory->Get("hde");
TH1F *he=(TH1F*)gDirectory->Get("he");
TH2F *hede=(TH2F*)gDirectory->Get("hede");

int nentries = (Int_t)t1->GetEntries();
printf("nentries=%d\n",nentries);

for (int i=0;i<nentries;i++) {

  t1->GetEntry(i);

  // integrate baseline o get baseline value
  n_baseline_chan = BASELINE_END-BASELINE_START;
  baseline_sum=0;
  for (int j=BASELINE_START;j<BASELINE_END;j++)
  {
    baseline_sum=baseline_sum+www[j];
    //printf("%d %d %d\n",j,www[j],baseline_sum);
  }
  baseline = (float)baseline_sum/(float)n_baseline_chan;
  //baseline=2550;
    ULong64_t timestamp,extended;
  // short integral
  short_int = 0;
  for (int j=SHORT_START;j<SHORT_END;j++) short_int = short_int -(www[j]-baseline);

  // long integral
  long_int = 0;
  for (int j=LONG_START;j<LONG_END;j++) long_int = long_int -(www[j]-baseline);

  //printf("Event: %d Baseline: %f n_baseline_chan: %d Short: %d Long: %d \n",i,baseline,n_baseline_chan,short_int, long_int);

  short_int=short_int/3.;
  long_int=long_int/3.;

  // test the cut
  if (cutg->IsInside(long_int,short_int)) incut[i]=true; else incut[i]=false;

  hde->Fill(short_int);
  he->Fill(long_int);
  //if (incut[i]) hede->Fill(long_int,short_int);
  hede->Fill(long_int,short_int);

  }

cutg->Draw();
cutg->Print();
c1->Update();
c1->Draw();

}

// ++++++++++++++++++++++++++++++++++++++++++++++++++++++
// Fill time histograms from cuts on 2D histogram
// ++++++++++++++++++++++++++++++++++++++++++++++++++++++
void thist(int start_channel) {

int integral=0;
double event_time;  // in sec

// Functions for fitting
TF1 *decay_function = new TF1("decay","[0]*exp(-[1]*x)+[2]", 0.,duration/tdiv);
TF1 *growth_function = new TF1("growth","[0]*(1.-exp(-[1]*x))+[2]*x", 0.,duration/tdiv);
TF1 *growth_function2 = new TF1("growth2","[0]*(1.-exp(-[1]*x))+[2]*(1.-exp(-[3]*x))+[4]*x", 0.,duration/tdiv);
```

```
make_thists();
TTree *t1=(TTree*)gDirectory->Get("t1");
TCanvas                 *c3=(TCanvas*)gROOT->GetListOfCanvases()-
>FindObject("c3");
TH1D *decay=(TH1D*)gDirectory->Get("decay");
TH1D *growth=(TH1D*)gDirectory->Get("growth");

int nentries = (Int_t)t1->GetEntries();
printf("nentries=%d\n",nentries);

// Fill the decay histogram
for (int i=0;i<nentries;i++) {
   t1->GetEntry(i);

   // test to see if event made the cut
   if (incut[i]) {

event_time=((double)timestamp+(double)extended*pow(2,31))*2.e-9;
      decay->Fill(event_time/tdiv);
   }

   //printf("%d    %s    %llX    %llX        %f\n",i,incut[i]?"in":"out",
timestamp,extended,event_time);

}

// Fill the growth curve
for (int i=start_channel;i<NUM_TIME_BINS;i++) {
   integral=integral+decay->GetBinContent(i);
   growth->SetBinContent(i-start_channel, integral);
}

c3->Update();
c3->Draw();

// create histogram of clock time vs timestamp
TCanvas *c5 = new TCanvas("c5","c5",1000,10,700,1200);
TH2F *diff=new TH2F("clocks", "",500,0,30,500,0,30);
diff->Draw();

int jj=0;
for (int i=0;i<nentries;i++) {
   t1->GetEntry(i);
   event_time=((double)timestamp+(double)extended*pow(2,31))*2.e-
9;

   //if (clocks/1000.>0.7 && clocks/1000.<0.9) {
      //printf("ev=%hu    wsize=%hu    timestamp=%llu    extended=%llu
clocks=%llu\n",ev,wsize,timestamp,extended,clocks);
     // jj++;
   //}

   diff->Fill(event_time,clocks/1000.);

}
printf("jj=%d\n",jj);

c5->Update();
c5->Draw();

}

// ++++++++++++++++++++++++++++++++++++++++++++++++++++++
// Plot the waveform for a single event
// Usage:  wave( event_number)
//
// Requires saved WAVES
// ++++++++++++++++++++++++++++++++++++++++++++++++++++++
void wave( int i=0) {

make_whists();
TTree *t1=(TTree*)gDirectory->Get("t1");
TCanvas                 *c2=(TCanvas*)gROOT->GetListOfCanvases()-
>FindObject("c2");
TH1F *h2=(TH1F*)gDirectory->Get("h2");

int nentries = (Int_t)t1->GetEntries();
```

```
printf("nentries=%d\n",nentries);

t1->GetEntry(i);
printf("b=%hu ch=%hu ev=%hu wsize=%hu timestamp=%llu extended=%llu \n",b, ch,ev,wsize,timestamp,extended);
printf("Eshort=%d Elong=%d \n",Eshort,Elong);
for (int j=0;j<400;j++) printf("%u ",www[j]);
for (int j=0;j<400;j++) h2->SetBinContent(j+1,www[j]); // bin 0 is underflow

h2->Draw();

}

// ++++++++++++++++++++++++++++++++++++++++++++++++++
// Plot the waveforms for multiple events
// Usage: waves(start_event_number, end_event_number)
//
// Requires saved WAVES
// ++++++++++++++++++++++++++++++++++++++++++++++++++
void waves( int i1=0, int i2=0) {

make_whists();
TTree *t1=(TTree*)gDirectory->Get("t1");
TCanvas *c2=(TCanvas*)gROOT->GetListOfCanvases()->FindObject("c2");
TH1F *h2=(TH1F*)gDirectory->Get("h2");

int nentries = (Int_t)t1->GetEntries();
printf("nentries=%d\n",nentries);

for (int i=i1;i<i2;i++) {

  t1->GetEntry(i);
  printf("Pulse #%d b=%hu ch=%hu ev=%hu wsize=%hu timestamp=%llu extended=%llu \n",i,b,ch,ev,wsize,timestamp,extended);
  printf("Eshort=%d Elong=%d \n",Eshort,Elong);
  for (int j=0;j<400;j++) printf("%u ",www[j]);
  for (int j=0;j<400;j++) h2->SetBinContent(j+1,www[j]);
// bin 0 is underflow

  h2->Draw();
  c2->Update();
  printf("\nEnd Pulse #%d (Press ENTER to continue)\n",i);
  getchar();
  }


}
```

R e f e r e n c e s

[1] R.G. Pizzone, R. Spartá, C.A. Bertulani, *et. al*, The Astrophysical Journal **786**, 112 (2014).
[2] L. Sbordone, *et. al*, Astronomy and Astrophysics **522**, A26 (2010).
[3] M. Popspelov and J. Pradler, Annual Review of Nuclear and Particle Science **60**, 539-568 (2010).
[4] A. Koning, S. Hilaire, and S. Goriely, The European Physical Journal A **59**, (2023).
[5] S.N. Abramovich, B.Ya. Guzhovskij, V.A. Zherebtsov, and A.G. Zvenigorodskij, International Nuclear Data Committee Report INDC(CCP)-326/L+F, (1991).
[6] M. Yuly, A. Bo, S. Plymale, D. Vara, C. Freeman, G. Marcus, S. Padalino, "A Phoswich Detector System for Nuclear Measurements using ICF and TNSA," (2025) (unpublished).
[7] A. Schwemmlein, Ph. D. Thesis, University of Rochester, 2021.
[8] K. Cook, B.S. Thesis, Houghton College, 2019.
[9] J. Opelka, et al., Radiation Physics and Chemistry **161**, 48-54 (1979).
[10] International Atomic Energy Agency, International Atomic Energy Agency, (2020).
[11] I. Wiedenhoever, NSAC Long-Range Plan Town Hall Meeting on Nuclear Structure, Reactions and Astrophysics, Nov 14-16, (2022).
[12] M. Yuly, A. Bo, A. Belanger, O. Fall, S. Padalino, C. Freeman, "Nuclear physics using ultrafast high-power laser ion acceleration," (2024) (unpublished).
[13] A. Schwemmlein, et al., Review of Scientific Instruments **97**, (2026).
[14] LLE, NSF OPAL Flagship Selection Report, WWW Document, https://rochester.app.box.com/s/rjnjfsczq597duurxta83h4mjhgtl6ul/file/1674677113497 (Accessed 4 May 2026), 2024.
[15] M. Yuly, S. Padalino, M. Coats, K. Cook, "A Phoswich Detector System to Measure the $^{3}H(t,\gamma)^{6}He$ Cross Section using ICF," (2017) (unpublished).
[16] T. Kowalewski, B.S. Thesis, Houghton College, 2021.
[17] M. Christensen, B.S. Thesis, Houghton College, 2022.
[18] M. Yuly, S. Padalino, A. Brown, A. Hotchkiss, C. Lei, A. Martin, "Trapping and detecting trace radioactive isotopes produced in ICF implosions," (2022) (unpublished).
[19] M. Yuly, S. Padalino, N. Harley, A. Hotchkiss, C. Lei, A. Martin, "A new technique for measuring light ion nuclear reactions using TNSA," (2023) (unpublished).
[20] A. Martin, B.S. Thesis, Houghton University, 2024.
[21] S. Agostinelli, et al., Nuclear Instruments and Methods in Physics Research Section a Accelerators Spectrometers Detectors and Associated Equipment **506**, 250–303 (2003).
[22] Bethe, H., Zur Theorie des Durchgangs schneller Korpuskularstrahlen durch Materie. Ann. Phys., 397: 325-400 (1930).
[23] Bethe, H. Bremsformel für Elektronen relativistischer Geschwindigkeit. *Z. Physik* **76**, 293–299 (1932).
[24] Bloch, F. Bremsvermögen von Atomen mit mehreren Elektronen. *Z. Physik* **81**, 363–376 (1933).
[25] LaserNetUS, WWW Document, https://lasernetus.org/facilities/omega-ep (Accessed 4 May 2026).

[26] C. Lei, B.S. Thesis, Houghton University, 2024.
[27] M.M. Markowitz, and D.A. Boryta, Journal of Chemical & Engineering Data **7**, 586–591 (1962).
[28] F. James, and M. Roos, CERN program library long writeup D506, 1998.
[29] Brun, R. and Rademakers, F., Nuclear Instruments and Methods in Physics Research **389**, 81–86 (1997).